Dynamic composite hydrogels of gelatin methacryloyl (GelMA) with supramolecular fibers for tissue engineering applications

Anaïs Chalard, Harrison Porritt, Emily Lam Po Tang, Andrew Taberner, Annika Winbo, Amatul Ahmad, Juliette Fitremann, Jenny Malmström

Biomaterials Advances 163 (2024) 213957

Contents lists available at ScienceDirect

Biomaterials Advances

journal homepage: www.journals.elsevier.com/materials-science-and-engineering-c

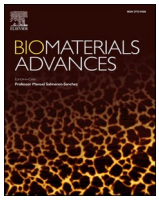

Dynamic composite hydrogels of gelatin methacryloyl (GelMA) with supramolecular fibers for tissue engineering applications

Anaïs E. Chalard [a,b], Harrison Porritt [a,b], Emily J. Lam Po Tang [c], Andrew J. Taberner [c,d], Annika Winbo [e,f], Amatul M. Ahmad [e], Juliette Fitremann [g], Jenny Malmström [a,b,*]

[a] Department of Chemical and Materials Engineering, Faculty of Engineering, The University of Auckland, Auckland, New Zealand
[b] The MacDiarmid Institute for Advanced Materials and Nanotechnology, Wellington, New Zealand
[c] The Auckland Bioengineering Institute (ABI), The University of Auckland, Auckland, New Zealand
[d] Department of Engineering Science and Biomedical Engineering, Faculty of Engineering, The University of Auckland, Auckland, New Zealand
[e] Department of Physiology, The University of Auckland, Auckland, New Zealand
[f] Manaaki Manawa Centre for Heart Research, The University of Auckland, Auckland, New Zealand
[g] Laboratoire Softmat, Université de Toulouse, CNRS UMR 5623, Université Toulouse III – Paul Sabatier, Toulouse, France

ARTICLE INFO

Keywords:
Biomaterial
Composite hydrogel
Supramolecular fibers
Galactonamide
GelMA
Mechanical characterization
Cardiac fibroblasts

ABSTRACT

In the field of tissue engineering, there is a growing need for biomaterials with structural properties that replicate the native characteristics of the extracellular matrix (ECM). It is important to include fibrous structures into ECM mimics, especially when constructing scar models. Additionally, including a dynamic aspect to cell-laden biomaterials is particularly interesting, since native ECM is constantly reshaped by cells. Composite hydrogels are developed to bring different combinations of structures and properties to a scaffold by using different types and sources of materials. In this work, we aimed to combine gelatin methacryloyl (GelMA) with biocompatible supramolecular fibers made of a small self-assembling sugar-derived molecule (*N*-heptyl-D-galactonamide, GalC7). The GalC7 fibers were directly grown in the GelMA through a thermal process, and it was shown that the presence of the fibrous network increased the Young's modulus of GelMA. Due to the non-covalent interactions that govern the self-assembly, these fibers were observed to dissolve over time, leading to a dynamic softening of the composite gels. Cardiac fibroblast cells were successfully encapsulated into composite gels for 7 days, showing excellent biocompatibility and fibroblasts extending in an elongated morphology, most likely in the channels left by the fibers after their degradation. These novel composite hydrogels present unique properties and could be used as tools to study biological processes such as fibrosis, vascularization and invasion.

1. Introduction

Tissue engineering promises to revolutionize medicine by replicating artificial tissues for transplantation, and by offering robust tissue models to study the mechanisms and behaviors of various cell types in different environments, to better understand both healthy and disease states. Providing an environment as similar as possible to native tissues is crucial to ensure the accuracy of these in vitro models, and replicating the extracellular matrix (ECM) surrounding living cells is one of tissue engineering's (TE) big challenges. [1–4] Hydrogels are a class of materials that reproduce several aspects of the properties of ECM in vitro, especially providing a highly hydrated environment that can act as support for cells to grow in or onto. Hydrogels can be made of natural or synthetic polymers, and are usually composed of at least 90 % of water, which makes them perfect for culturing cells in. [5] Gelatin methacryloyl (GelMA) is a good example of such a material, which has been used in a widespread range of TE applications. [6–8] GelMA is composed of gelatin, which is a denatured version of collagen, itself a main component of ECM. This renders GelMA biocompatible and provides biological cues, such as the integrin-binding motifs that contribute to cell attachment. [7] GelMA is easily synthesized and prepared in the laboratory [9], and the hydrogels are usually photo-crosslinked using photoinitiators sensitive to ultra-violet (UV) or visible light. The latter is increasingly favored as it has been shown that UV light can be detrimental for cell survival in the case of cell encapsulation in 3D culture. [10] Consequently, visible light crosslinking of GelMA using lithium

* Corresponding author at: Department of Chemical and Materials Engineering, Faculty of Engineering, The University of Auckland, Auckland, New Zealand.
E-mail address: j.malmstrom@auckland.ac.nz (J. Malmström).

https://doi.org/10.1016/j.bioadv.2024.213957
Received 26 March 2024; Received in revised form 4 July 2024; Accepted 10 July 2024
Available online 14 July 2024

acylphosphinate (LAP) [11], eosin Y [12,13], or ruthenium-based [14] photoinitiators is increasingly employed for TE applications. By controlling the crosslinking of GelMA, it is possible to precisely tune and even pattern its mechanical properties to replicate those of biological tissues. [12]

It is never possible to completely replicate the various structural and mechanical properties of biological tissues with a single biomaterial. For instance, an aspect that is more intricate to reproduce is the hierarchical structure in native ECM, organized between different forms and types of proteins, polysaccharides and glycoproteins. This type of organization is quite relevant in the case of scar tissue, where the excessive deposition of ECM proteins, in particular collagen, ends up forming bundles of proteins that provide enhanced tissue stiffness as well as potential cell guidance along aligned protein fibers. [15–17] This is why composite biomaterials that combine complementary properties of different materials have emerged in the field of TE over the years. [18–20] Cardiac scar tissue engineering, in particular, relies on composite materials to provide scaffolds with a good biocompatibility while displaying relevant mechanical properties, anisotropic structures, or electrically conductive properties, which are key factors required to properly mimic cardiac tissue. [4,21] In the case of scar tissue, a composite gel would ideally present larger aligned fibrous structures – to mimic the collagen fiber bundles onto which cells can attach and grow, as well as to enhance the mechanical properties of the scaffold – encapsulated into a highly hydrated and porous hydrogel matrix to promote cell survival and proliferation. Many studies have thus tried to provide such fibrillar structural properties to cell culture biomaterials. Common ways of doing so are with the use of electrospun fibers from different types of materials, synthetic or natural. [22–25] These fibers can be easily incorporated into hydrogel scaffolds, allowing relatively good control over their structure, which can include anisotropy for cell alignment. Moreover, the fibers provide support for the cells to attach and spread. However, the electrospinning of fibers often involves the use of toxic solvents to dissolve the primary materials, and some electrospun fibers require a subsequent additional cell adhesion functionalization for the cells to grow properly. Composite materials can also be produced by combining different fibrous proteins such as collagen, fibrin or cellulose [26–28], which allows the materials to only contain natural and biocompatible components. However, achieving good control over the protein's structure, or obtaining larger fiber sizes is more complicated with natural proteins compared to synthetic materials. Supramolecular self-assembling molecules are gaining more and more interest in TE, where they are being used as pure materials or integrated into composite scaffolds. [29–33] The self-assembly of supramolecular materials can be controlled and tailored by changes in, for example, pH, temperature and solubility. One of the main advantages of supramolecular materials is their potential reversibility, which can create dynamic materials. [34,35] For instance, self-assembling peptides such as fluorenylmethoxycarbonyl diphenylalanine (Fmoc-FF) are often used as a supramolecular building block, and composite gels of gelatin and Fmoc-FF have been demonstrated. [36] Another example of a supramolecular/hydrogel composite is one where collagen hydrogels were combined with gels from gluco-nucleo-lipids with fluorinated carbon chains driving the self-assembly. The resulting gels were found to be biocompatible and to manifest improved mechanical properties suitable for bone tissue engineering. [37]

In this work, we aim to combine GelMA with a low-molecular weight gelator (LMWG), *N*-heptyl-galactonamide (GalC7), to integrate a fibrous network inside the modified protein hydrogel.

GalC7 hydrogels are formed by cooling down an aqueous solution of GalC7 from 100 °C to room temperature (RT). During cooling, the molecules self-assemble through non-covalent interactions to form a network of wide and long ribbon-like fibers, retaining water. The GalC7 molecule was introduced recently, for use as a biomaterial. [38] It was demonstrated that this pure, synthetic molecule was suitable to create hydrogels, and that the synthetic origin avoids the problem of batch reproducibility encountered in the case of polymers, due to the polydispersity of the polymers, whether natural or synthetic. Thanks to the non-covalent nature of the network and its very low density, better cell penetration within the material was also noted. [38] In the previous studies using GalC7, it has been shown that the GalC7 molecule forms biocompatible hydrogels that could be used as scaffolds for neural cell culture. Moreover, the material can be 3D-printed. [38–40] The pure GalC7 hydrogels allowed the 3D culture of neural stem cells for up to 7 days in vitro, after which the cells showed signs of differentiation into glial cells and neurons. [38] Neurites were found to grow very long in straight directions, and it can be hypothesized that the ribbon-like structure of the fibers provided support for the cells to grow along. However, pure GalC7 hydrogels are very fragile and affected by syneresis, which is the irreversible expulsion of water from the fibrous network upon a mechanical strain. [38] By integrating the supramolecular GalC7 fibers into a GelMA matrix used for 3D cell culture, we aim to add new properties to the composite hydrogels, in addition to the excellent biocompatibility and control over mechanical properties that GelMA provides. We aim for the fibers that can provide support and guidance to proliferating cells, to enhance the overall scaffold's stiffness by reinforcing GelMA with a fibrous network, and to bring a dynamic aspect to the composite by allowing the disintegration of the supramolecular fibers over time.

This article describes methods to incorporate supramolecular GalC7 fibers into a GelMA matrix, thus creating a composite scaffold. This novel biomaterial was then extensively characterized using various techniques to confirm the incorporation of the fibers into the GelMA, to study the dynamic nature of the constructs with fiber degradation over time, and to measure their mechanical properties. Finally, 3D cell culture trials were performed using cardiac fibroblast cells encapsulated into the composite gels.

2. Experimental section

2.1. Materials

All the solutions were prepared with Ultrapure/Type 1 water sourced from a Milli-Q Direct 8 water purification system with a resistivity of 18.2 MΩ cm. Gelatin, methacrylic anhydride, tris(2,2-bipyridyl) dichlororuthenium(II) hexahydrate (Ru), sodium persulfalte (SPS), (3-aminopropyl) triethoxysilane, 50 % *v*/v glutaraldehyde solution, dichlorodimethylsilane, and cellulose dialysis tubing were all purchased from Sigma-Aldrich (Auckland, New Zealand). Sodium azide was from Scharlau. Gibco phosphate buffer saline (PBS) tablets were purchased from Life Technologies (Auckland, New Zealand). *N*-heptyl-galactonamide (GalC7) was purchased from Innov'Orga (Reims, France). Ethanol, acetone, and toluene (AR grade) were purchased from ECP Ltd. (Auckland, New Zealand). Polypropylene centrifuge tubes, glass vials, and crimp-top septum caps were purchased from Interlab Ltd. (Wellington, New Zealand). Silicon (Si) wafers (100 orientation, P-type, boron doped) were purchased from University Wafers (Boston, MA, USA).

2.2. GelMA synthesis

GelMA was synthesized according to Loessner et al.'s protocol [9]. Briefly, gelatin (from porcine skin, gel strength 300, Type A) was dissolved at a concentration of 10 wt% in PBS and heated at 50 °C for 1 h. Methacrylic anhydride (0.6 g per g of gelatin) was added dropwise to the reaction mixture, which was then left to react under stirring for 3 h at 50 °C. The reaction mixture was centrifuged to remove the unreacted methacrylic anhydride, and the supernatant was diluted in twice its volume of warm PBS and transferred into dialysis tubing (cellulose tubing, MWCO 12,400 kDa). The GelMA was then dialyzed against Type 1 water for 7 days at 40 °C. After purification, the resulting GelMA was freeze-dried and stored at −20 °C.

2.3. Determination of the degree of functionalization of GelMA

Following Zatorski et al.'s protocol [41], a ninhydrin assay was performed to determine the degree of functionalization of the synthesized GelMA. Briefly, a 10 mg/ml gelatin solution in PBS was prepared and diluted at (90, 80, 70, 60, 50, 40, 30, 20 and 10) % in PBS. A GelMA solution in PBS at a concentration (C_{nom}) of 10 g/l was also prepared. A ninhydrin solution in ethanol at 20 g/l was prepared. The gelatin or GelMA solutions were mixed with the ninhydrin solution (2.2 g/l final) at a 1:8 volume ratio (ninhydrin to gelatin/GelMA ratio) and heated at 70 °C (in the absence of stirring) for 12 min. The different solutions were pipetted in triplicates into the wells of a 96-well plate, and their absorbance at 570 nm was measured at room temperature (RT). A calibration curve was plotted to represent the absorbance of the gelatin against its concentration, and a linear fit was applied to concentrations between 2 g/l and 8 g/l. The "apparent concentration", C_{app}, of GelMA in g/l was then calculated by reporting the average absorbance of the GelMA solutions to the linear fit. The fraction of available amine functions (f) in the GelMA can be calculated as $f = \frac{C_{app}}{C_{nom}}$. The degree of functionalization was then calculated as: $DoF\ (\%) = 100 \times (1 - f)$.

2.4. Preparation of hydrophobic glass coverslips

Coverslips were cleaned by sonication for 15 min in acetone and exposure to UV ozone for 20 min on both sides. Around 20 µl of dichlorodimethylsilane was then applied to each side of the clean glass coverslips and left to react for approximately 2 min. The excess silane was wiped with a paper, and the functionalized coverslips were rinsed with Type 1 water.

2.5. Preparation of pure GelMA hydrogels

A 11 wt% GelMA solution in PBS was prepared by dissolving 110 mg of freeze-dried GelMA in 1 ml of PBS at 42 °C, then vortexed until fully homogenized and kept at 37 °C. A 8 mM Ru solution in PBS was prepared by dissolving 6 mg of tris(2,2-bipyridyl)dichlororuthenium(II) hexahydrate into 1 ml of PBS, and a 40 mM SPS solution in PBS was prepared by dissolving 9.5 mg of sodium persulfate into 1 ml of PBS.

To prepare the pre-gel solution, the three previous solutions were mixed together by adding together 180 µl of 11 wt% GelMA solution, 10 µl of the Ru solution, and 10 µl of the SPS solution. The final concentrations in GelMA, Ru and SPS are respectively 10 wt%, 0.4 mM and 2 mM.

To prepare a GelMA hydrogel, the different volumes of pre-gel solution were pipetted into a mold covered by a hydrophobic coverslip and crosslinked at room temperature (RT) under a white-light LED lamp (76.9 W/m^2 over the wavelength range of (400–450) nm, Mitre10, New Zealand) for the appropriate time: 4 min for the 10 µl, 70 µl circular molds, and the 30 µl dog bone molds for tensile tests, or 10 min (5 min on each side) for the 400 µl molds for compression tests samples.

2.6. Preparation of GalC7 solutions and hydrogels

To prepare GalC7 solutions or hydrogels at 0.45 wt% in Type 1 water or PBS, 4.5 mg of *N*-heptyl-galactonamide were added to 1 ml of Type 1 water or PBS in a sealed glass vial and heated at 105 °C in a block heater (Thermo Scientific Multi-Blok heater) until complete dissolution of the powder (<10 min). The supramolecular hydrogel formed upon cooling of the solution.

To control the fiber length of the GalC7 gels, the solution was slow cooled by being placed in an oven (Thermo Scientific, HeraTherm IMH60-S incubator) set at 100 °C, left for 5 min at this temperature, and then set at 37 °C and left to cool.

2.7. Preparation of composite hydrogels

2.7.1. Via embedding

0.45 wt% GalC7 hydrogels in water were prepared as described above by slow cooling in a 48-well culture plate covered with an aluminum sealing foil. Upon reaching 37 °C, the plate was taken out of the oven and the gels were rinsed 3 times overnight with 100 µl of PBS to remove small fibers and permeabilize the hydrogels. After removing the last rinse, 100 µl of pure GelMA pre-gel were added to the GalC7 hydrogels and left to penetrate the fibrous networks for 5 min at 37 °C. The samples were then placed under the white-light LED lamp and crosslinked for 4 min at RT.

2.7.2. Via direct mixing

A 0.45 wt% GalC7 solution was prepared in PBS as described above. After complete dissolution of the GalC7 powder, the corresponding amount of freeze-dried GelMA was added to the hot solution to make a 11 wt% solution of GelMA in the GalC7 solution and left at 105 °C in the block heater for 3 min until complete dissolution of the GelMA. The glass vial was then placed in the oven set at 100 °C, left for 5 min and then the oven was set at 37 °C and left to cool.

After reaching 37 °C, 180 µl of the GalC7 + GelMA solution were gently pipetted (with pipette tip cut at the end to enlarge the opening and reduce shear) and mixed with 10 µl of 8 mM Ru solution in PBS and 10 µl of SPS solution in PBS. The solution was homogenized by gentle aspiration with a cut pipette tip to minimize the coalescence of the supramolecular fibers. The corresponding amount of composite pre-gel was then placed in a mold and crosslinked under the white-light LED lamp for a corresponding time at RT.

2.8. Microscopy observations of the scaffolds

2.8.1. Confocal microscopy

Large pure GelMA and composite gels were prepared according to the protocol described above in molds with and internal diameter of 1 cm and a thickness of 1 mm (70 µl of pre-gel solution pipetted). The gels were crosslinked for 4 min under the white-light LED lamp. The gels were made right before the confocal observation and to prevent fiber degradation were not kept in any solvent. They were observed at 4× and 10× magnification with an Olympus FV1000 confocal microscope using laser reflection and light transmission techniques.

2.8.2. Cryo-SEM

Prior to the observation day, 70 µl composite and pure GelMA samples for cryo-SEM were prepared as described above and crosslinked for 4 min. All the gels were then soaked in 1 ml of PBS containing 0.02 % sodium azide for 1 h, after which the liquid was replaced for some gels while the others were kept without liquid until cryo-SEM sample preparation.

For cryo-SEM observations, the samples were cut and secured to sample holders using agar glue, prior to SEM imaging. They were then frozen in liquid nitrogen and transferred into the cryo-transfer system chamber (Gattan Alto 2500) under vacuum, where they were fractured at −140 °C, sublimed for 30 min at −90 °C and sputter-coated for 2 min with gold at −120 °C. Samples were subsequently imaged at −140 °C using a Philips XL-30 scanning electron microscope, with an acceleration voltage of 5 kV.

2.8.3. Fiber degradation study

Composite hydrogels were prepared in the 10 µl circular molds on a glass coverslip following the method described above. Once crosslinked, the gels were placed under the microscope in a 24-well plate containing the different solutions used for this experiment: 1 ml or 0.5 ml of PBS containing 0.02 wt% sodium azide, or 1 ml of solutions of GalC7 in PBS (also containing 0.02 wt% of sodium azide) at concentrations of 0.010 wt%, 0.025 wt% or 0.050 wt%. To make these solutions, the GalC7

powder was put with PBS in a vial and heated up to approximately 105 °C until full dissolution. The solution was then left to cool down on the bench at RT. In the microscope software (NIS-Elements, Nikon Instruments), time-lapse parameters were set to take images at intervals of 10, 20 or 30 min over 6 to 16 h depending on the conditions, and the exposure was kept constant during each experiment. ImageJ (Fiji) was then used to measure the fiber density over time on the microscopy pictures. To do so, each picture was converted to an 8-bit image. Next, a threshold was set and kept constant for all the images of a same experiment, thereby converting them to binary images. The percentage of black pixels was then measured on all images and normalized to the percentage of the first image. These percentages were then plotted against the time of acquisition.

2.9. Mechanical characterization of the hydrogels

2.9.1. Force indentation with Atomic Force Microscopy

The Young's modulus measurements of the hydrogel samples were performed on an MFP-3D Origin AFM (Asylum Research, Santa Barbara, USA) in a liquid environment at RT. Pre-calibrated silicon nitride cantilevers with spring constants ranging between 0.07 N/m and 0.08 N/m with a 5 μm glass bead at the tip (Novascan, USA) were used. The spring constant of each cantilever was precisely calibrated by the manufacturer beforehand, and its value was subsequently updated in the AFM software. Before each set of measurements, force-indentation curves were measured on a clean piece of silicon wafer in PBS to calibrate the DeflInvols value. Each hydrogel sample was put on a glass slide on the AFM stage, and a droplet of PBS was placed on top of the gel. The parameters used for measuring the elastic moduli of the hydrogels were adapted from Schillers et al. [42]: 100 force indentation curves over an area of 20 μm × 20 μm (= 1 force map) were recorded, typically with a scan rate of 0.7 Hz, travel range of 2 μm to 4 μm, tip velocity of 3 μm/s to 6 μm/s and trigger force of 2.5 nN to 5.0 nN. At least four force maps were recorded over the sample's area for each hydrogel. The resulting force maps were analyzed in the acquisition software, Asylum Research Software AR16 (version 16.10.211), operating in Igor Pro (version 6.38, WaveMetrics, USA), and the approach section of the curve was fitted with the Hertz model. [43] The equation used to fit force curves to approximate the Young's modulus of the sample was:

$$F_{app} = \frac{4}{3}\,\frac{E_s}{1-\vartheta_s^2}\,R^{1/2}\,d^{3/2}$$

with F_{app} the applied force in N, E_s the Young's modulus in Pa (N.m^{-2}), ϑ_s the sample's Poisson's ratio (dimensionless), R the radius of the bead in m, and d the depth of indentation in m. [44] The value of the Poisson's ratio of the gels was assumed to be 0.33. [45] A fit between 10 % and 90 % of the maximum applied force was used to quantify the Young's modulus of the hydrogel samples from the force-indentation curves. A histogram of the Young's modulus values was generated for each force map, and a Gaussian function fit to the data. This fit provided a mean value of the Young's modulus and the standard deviation (SD) for each force map. If some force curves within the force maps displayed irregular shapes or values, these were excluded from the fit by applying a mask that excluded force curves with a fit above or below a certain threshold of Young's modulus.

2.9.2. Compression testing

Samples for compression testing were prepared by crosslinking pure GelMA and composite pre-gel solutions in cylindrical black acrylamide molds of 5 mm of diameter and 10 mm of height between two hydrophobic coverslips. Approximately 400 μl of pre-gel was pipetted into the mold. The pre-gel was crosslinked for 5 min on each side under the while-light LED lamp to ensure homogeneous crosslinking throughout the height of the gels.

Fresh samples were directly tested on the machine, whereas swollen samples were kept in 2 ml of PBS overnight in the dark and at RT. The samples were tested with an Instron 5543 tensile testing machine (Instron, Norwood, USA) using a 50 N load cell. A pre-load of 0.02 N was applied to the samples, which were then compressed at a rate of 1 mm/min, three times until 20 % of compressive strain, and then a fourth time until failure. The compressive moduli of the samples were calculated by fitting the linear part of the stress-strain curves between 0 % and 10 % of compressive strain and extracting the slope of the fit.

2.9.3. Tensile testing

Composite and pure GelMA gel samples were prepared in PDMS dog bone molds (dimensions of 7 mm long, 1.5 mm wide, and 1 mm thick for the long axial portion, 30 μl of pre-gel solution inside) and crosslinked for 4 min under the white light LED according to the protocol described above.

Mechanical testing was performed on a custom-built device. The device included a panel mount load cell (LPM 200, Futek) for force measurement. This was paired with an amplifier (CSG110, Futek) to increase the output of the sensor from 1 mV/V to 10 mV/V. Actuation was provided by a worm screw motor with a 50 mm travel range and a resolution of 3.6 nm (M-227.50X, Physik Instrumente (PI)). Custom made attachments were constructed for the force sensor and motor to allow easy attachment of dog bone structures. The device was constructed using precision mechanical components (Microbench, Qioptic) allowing all the components of the system to be aligned with each other.

Code was implemented on an FPGA chip (PXI-7813R Virtex-II, NI) using the LabVIEW (2017) environment to read data from the force sensor and for control of the worm screw motor. The FPGA chip interfaced with the motor and force sensors via a R series CompactRIO expansion chassis (NI-9151) with a motor module (NI-9505) and an attached analogue input module (NI-9215). A custom-built LabVIEW program was used to control the displacement and strain rate of the sample during the tensile test and conduct cyclic tests of the constructs. The force and motor position were displayed to the user.

Mechanical tensile testing was performed using the device described above. The samples were placed in a bath of PBS to prevent drying throughout the experiment. The samples were stretched at 0.01 mms^{-1} to 20 % strain and the corresponding force measured at a sampling frequency of 1 kHz. The elastic modulus was calculated in the strain range of 0 % to 10 % on the stress-strain loading curve. The samples were also loaded/unloaded 3 times at a strain rate of 0.01 mms^{-1} to 20 % strain.

2.10. Culture of cardiac fibroblasts

Human ventricular cardiac fibroblasts (CF) (Lonza Bioscience) were cultured in a six well-plate lined with Geltrex™ (Gibco, A1569601) with media containing fibroblast basal media (FBM™), supplemented with 10 % fetal bovine serum (FBS), 0.1 % each of insulin, human fibroblast growth factor, and gentamicin x-1000 (Lonza Bioscience, FGM™-3 Cardiac Fibroblast Growth Medium-3 BulletKit™), and kept in an incubator at 37 °C and 5 % CO_2. For each encapsulation experiment, cells were prepared by washing with PBS and digested with trypsin for 5 min in an incubator. Digested CFs were added to 6 ml of media and spun down for 5 min at 200 RCF. Cells were counted using trypan blue after discarding the supernatant and replacing it with 1 ml of media. The appropriate volume of cells plus media was spun down again to get a final cell density of 1.25 million cells/ml when added to the pre-gel. The supernatant was discarded and 180 μl of the GalC7 + GelMA solution in PBS held at 37 °C, and 10 μl of 8 mM Ru solution in PBS and 10 μl of SPS solution in PBS which was sterile-filtered using a 0.22 μm polyethersulfone filter (Sigma-Aldrich), was gently mixed into the cells by aspirating it up and down. The resulting cell suspension, in pre-gel solution, was pipetted into the 10 μl mold on a glutaraldehyde-functionalized glass coverslip, covered by a hydrophobic glass coverslip and crosslinked for 4 min under the white-light LED lamp. The

coverslip and mold were then removed, and the crosslinked gel attached to the coverslip was placed in a 12-well plate. 500 µl of fibroblast basal media supplemented with 0.025 wt% GalC7 was added to each well. The media was prepared by adding 200 µl 1.25 wt% GalC7 dissolved in PBS then sterile filtered using a 0.22 µm polyethersulfone filter (Sigma-Aldrich), into 10 ml of fibroblast basal media. The media was changed 24 hour post-encapsulation and every 48 h after that.

2.10.1. Cell viability

Live/dead assay containing green (Calcein, AM, cellpermeant dye, ex/em 488 nm/515 nm) and red (BOBO-3 Iodide, ex/em 570 nm/602 nm) dyes (ThermoFisher Scientific) were thawed and mixed. Cell medium was discarded from each well plate, and 300 µl of FBM as well as 100 µl of live/dead cell assay were added to each well and kept at 37 °C for 15 min before imaging. Imaging was performed using an EVOS M5000 microscope (ThermoFisher Scientific). Images of the cells were taken at wavelengths of 600 nm (Texas Red-X) and 500 nm (GFP green), and the images were merged using the EVOS software.

2.10.2. Immunostaining

After seven days in culture, the gels were washed twice with PBS and fixed, using 4 % paraformaldehyde (Sigma Aldrich) for 15 min. Afterwards, gels were washed with PBS again and kept in PBS plus 0.25 % sodium azide until staining. For staining, each gel was washed twice with PBS followed by adding 1 ml of 0.25 % triton-X 100 (Sigma-Aldrich) in PBS to each of the wells and left for 30 min on a rocker. Triton-X 100 was removed and replaced with 0.25 % triton-X 100 with 4 % donkey serum (DS) (Merck Life Science Ltd. New Zealand, Sigma-Aldrich, D9663) as a blocking agent, and left for 1 h on the rocker. After the Triton-X 100, 5 µl of Alexa Fluor™ 568 Phalloidin (Thermo Fisher New Zealand, A22282) in methanol was added to 195 µl of 0.25 % triton-X 100, 4 % DS, to give a final phalloidin concentration of 1 unit/ml or 33 nM. This was left in the fridge at 2 °C for 24 h, followed by washing with 1 ml of PBS twice for 15 min each. PBS was replaced and gels were stored in the fridge for another 24 h. To mount the gels, a drop of DAPI containing mounting stain (Thermo Fisher Scientific New Zealand Ltd., Prolong Gold Antifade Reagent 5 × 2, P36935) was placed onto a glass slide, and the gel attached to the glass coverslip was inverted and placed onto the DAPI mounting stain. This was then sealed with nail polish, incubated for a minimum of 30 min, and imaged using an EVOS FV1000 microscope. Samples were imaged at 405 nm and 568 nm for DAPI and phalloidin, respectively. Stacks of images were taken at roughly 3 µm apart for the length of the gel and merged using ImageJ (Fiji) to compile the final images.

3. Results and discussion

3.1. Fabrication of the composite hydrogels

To design methods to create composite hydrogels, it is important to note that GalC7 only dissolves in a hot aqueous solution and the supramolecular fibers form through slow cooling, while GelMA gels through the irradiation of light in the presence of photoinitiators. For applications in 3D cell culture, cells can only be added to the solution at 37 °C. Considering these limitations, two approaches were explored to create a composite supramolecular fiber-containing GelMA gel in which cells can also be embedded.

In the first method, a GalC7 hydrogel is first prepared, rinsed several times to permeabilize the network by partial dissolution of GalC7 and/or extraction of unbound small fibers. Then it is embedded into GelMA, as described into Fig. 1A. The slow cooling step to form the galactonamide gel is crucial as it has previously been reported that the slower the cooling, the longer the fiber length. [38]

This method was efficient to obtain a dense supramolecular fibrous network embedded inside the GelMA matrix, as can been seen on the microscopy image on Fig. 1C. However, it is challenging to get a

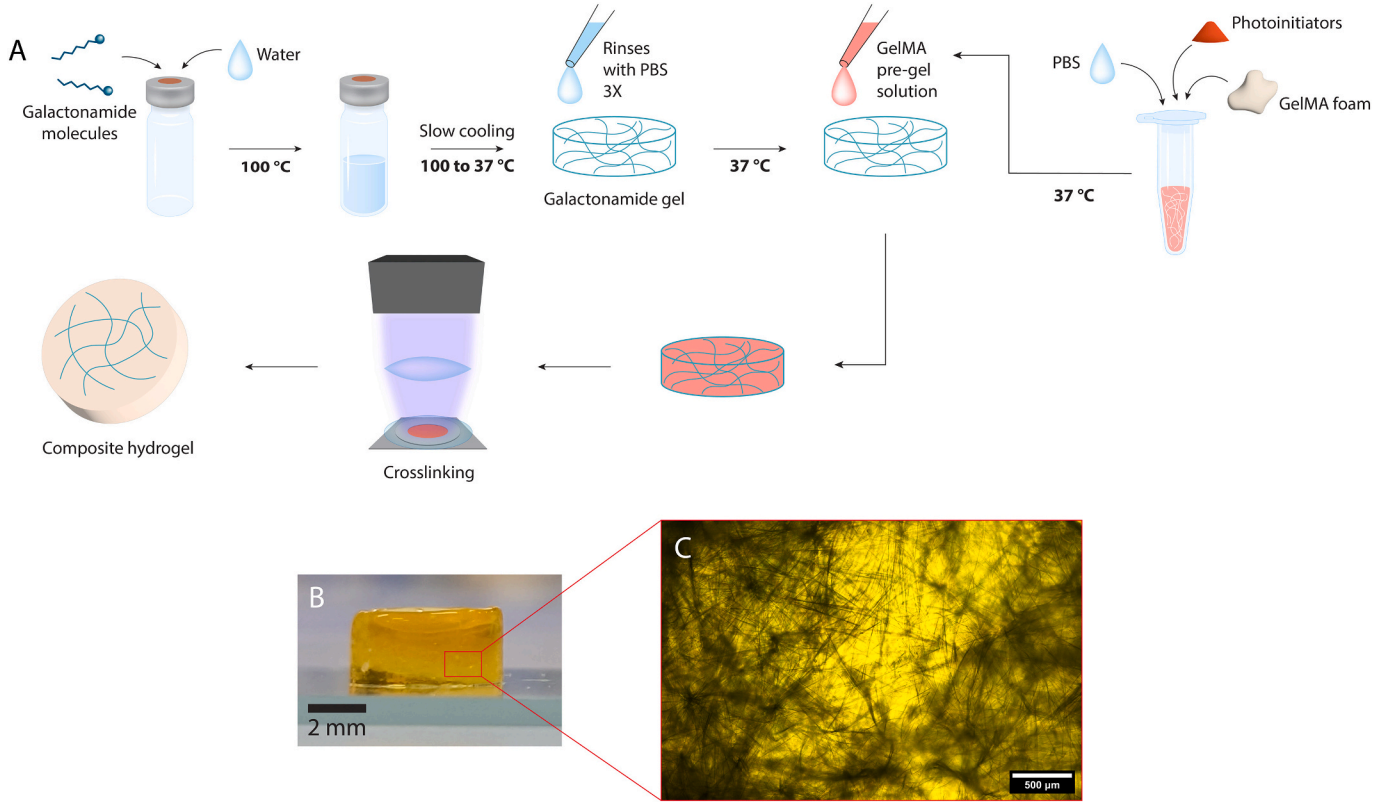

Fig. 1. A) Scheme describing the fabrication of GelMA-GalC7 composite gels through the embedding method. B) Picture of an embedded composite hydrogel (scale bar: 2 mm). C) Optical microscopy image of the fibrous network inside the composite gel (scale bar: 500 µm).

homogenous distribution of the fibers in the GelMA gel. Fig. 1B highlights that the fibrous network does not distribute well within the GelMA, but remains as a dense mat. Thus, this method is useful for applications where a high concentration of supramolecular fibers is desired within GelMA. Suitable applications would be those that require very fibrous, or layered, tissue models, such as cartilage or cortical/trabecular bone. The limitation with this method is that the three washes with PBS to permeate the fibrous network are done overnight, which requires 3 days just to permeate the network. In addition, while GelMA can penetrate the fiber mesh, it may be challenging to seed cells into the fibrous network, and the method is certainly not suitable as culture environments for larger constructs, such as organoids.

In light of these challenges, a second method was developed to directly grow the fibers of GalC7 inside the GelMA solution. Our hypothesis was that this will allow for a sparser and better distributed network of fibers. To achieve this, we prepared a 0.45 wt% solution of GalC7 in PBS by dissolving the solid galactonamide at 100 °C in a sealed vial, to prevent boiling. Once the GalC7 was fully dissolved, GelMA was added and dissolved at 100 °C. The resulting solution (11 wt% GelMA, 0.45 wt% GalC7 (with respect to water)) was placed in an oven and slowly cooled down from 100 °C to 37 °C for long supramolecular fibers to form (Fig. 2A). After the cooling ramp was finished, the fiber-containing GelMA solution was mixed with a solution of tris(2,2-bipyridyl)dichlororuthenium(II) hexahydrate (Ru) and sodium persulfate (SPS) photoinitiators to form the pre-gel solution. Cells can be included at this step but were omitted for gel characterization. The solution was pipetted into a mold and exposed to visible light for the required amount of time to crosslink and form the final composite hydrogel.

As can be seen on Fig. 2B and C, a network of GalC7 fibers was obtained inside the GelMA matrix, showing that the supramolecular self-assembly and fiber growth can still progress in the presence of GelMA. Composite hydrogels with an excellent distribution of fibers can be obtained with this method. The fibers do not appear as straight and long as those in the embedded gels (Fig. 1C). This could be because pipetting is required to mix the solutions together, hence resulting in some fiber breakage and disorganization inside the composite, or due to a disruption of the self-assembly process in presence of GelMA, when compared to in pure water. However, compared to the method where pure GalC7 gels are embedded into the GelMA, the direct fiber growth method is more straightforward and requires less preparation time, mainly due to the absence of overnight washes. This method also has the potential to create gels with different fiber concentrations to suit different tissue engineering applications. While the fibers can only form from a relatively high concentration of GalC7, they can be diluted further at the step when photoinitiators are added. In this method, GelMA must be heated up to 100 °C, and we have confirmed that this does not impact on the resulting mechanical properties of the GelMA gel (Fig. S1). Considering the success of the direct fiber growth method, we decided to fully characterize these composite hydrogels.

3.1.1. *Characterization of the fiber growth into GelMA*

To tailor the fiber length within GelMA, it is crucial to understand the fabrication process. To understand what temperature needs to be reached during the cooling ramp to obtain long fibers, we investigated fiber development during that step. For this study, six samples of GelMA + GalC7 solution (respectively 11 wt% and 0.45 wt%) were prepared and put in the oven at 100 °C. The oven was then set to 37 °C and allowed to cool, while the temperature was monitored. While cooling down, a sample was taken out at each temperature point (90 °C, 80 °C, 70 °C, 60 °C, 50 °C and 40 °C, see Fig. S2 for temperature vs. time) and directly placed at 37 °C. A sample of each solution was then observed in bright field microscopy at RT (Fig. 3). If taken out of the ramp at the early stages of cooling, 90 °C, 80 °C or 70 °C, only short and highly branched fibers were formed. Several repeats were made for 60 °C and 50 °C showing different fiber aspects, i.e. short or long fibers. This shows that this temperature zone is a transition stage, where the tipping point between short and long fibers sits. This result is in accordance with previous differential scanning calorimetry (DSC) results obtained for the GalC7 molecule, which showed that the transition temperature from

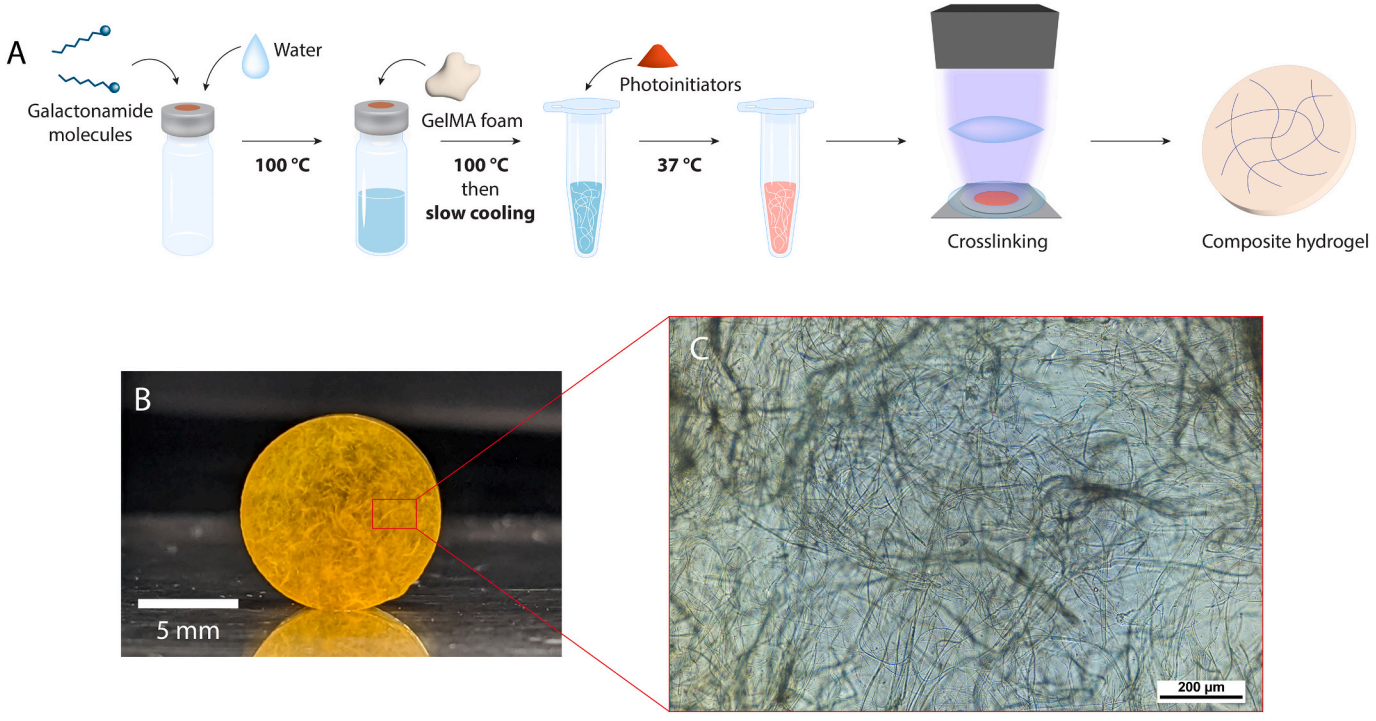

Fig. 2. A) Scheme describing the fabrication of GelMA-GalC7 composite gels through the direct growth of GalC7 fibers into the GelMA. B) Picture of a composite hydrogel prepared with the direct fiber growth method (sample used for compression tests, scale bar: 5 mm). C) Optical microscopy image of the fibrous network inside the composite hydrogel (scale bar: 200 µm).

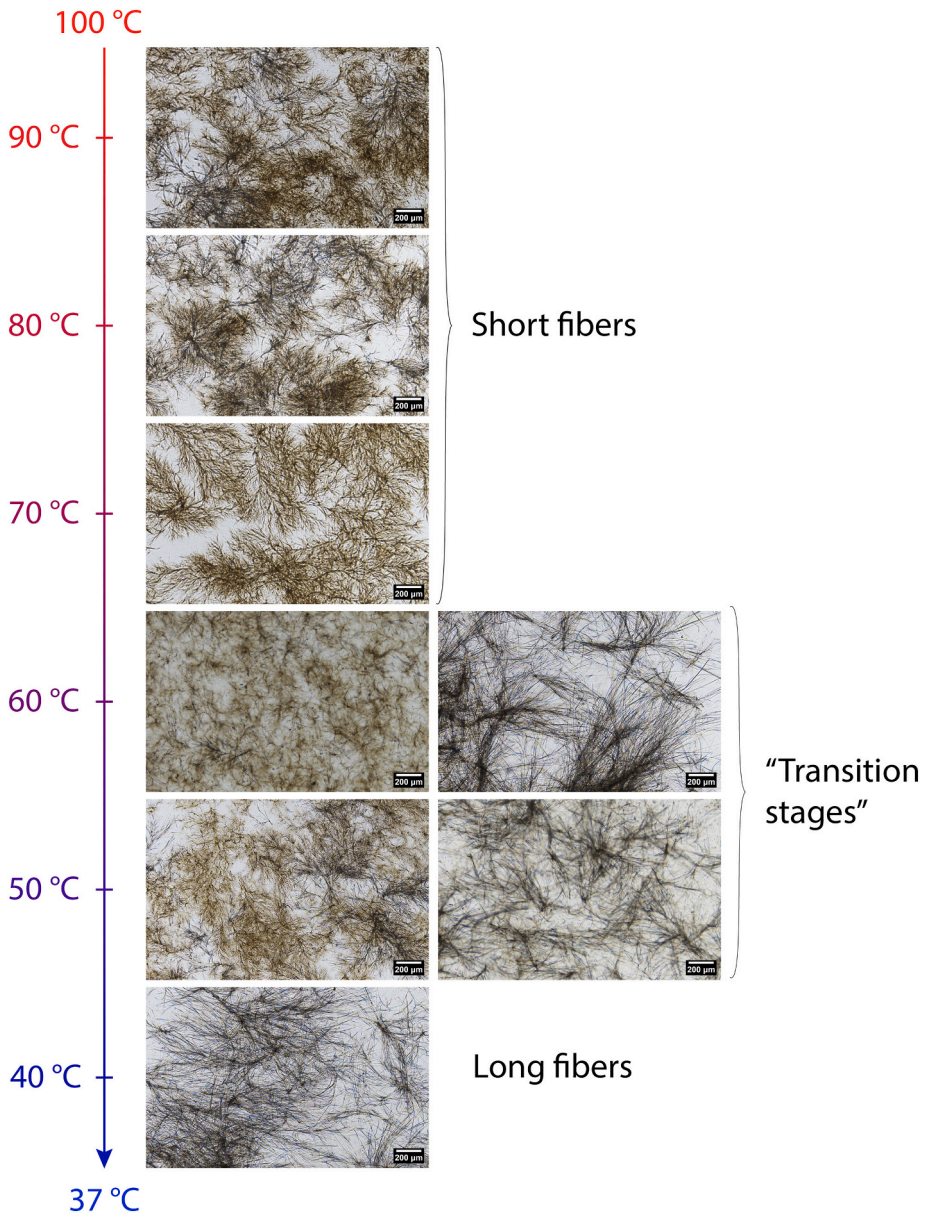

Fig. 3. Optical microscopy images showing the fiber aspect when the composite gels are taken out of the oven at different temperatures of the ramp (scale bar: 200 μm).

solution to gel ($T_{sol\text{-}gel}$) is 58 °C for GalC7. [38] This is the temperature at which the fibrous network has grown enough to retain the water and form the gel, which means that 58 °C is a critical temperature for fiber formation and it needs to be reached during the ramp for the fibers to have a significant length.

To further characterize fiber morphology inside the composite hydrogels, crosslinked samples were observed with confocal microscopy with laser reflection technique (Fig. 4). Indeed, the supramolecular fibers, and in particular the large ones, are not transparent to the laser, which makes them visible in confocal microscopy without the need of staining (Fig. 4A). The supramolecular fibers are thus clearly visible in these images, both in laser reflection mode and in bright field, and they reveal a dense network of long fibers. Surprisingly though, the fibers that are observed in laser reflection mode and bright field are not the same, as the fibers generally do not overlap on the merged image, especially for the large and wide fibers (Fig. 4C). The orientation of the ribbon-like fibers under the objective might be the reason for this result. It is likely that only the wide fibers, that lay flat and parallel to the focal plane might be reflecting the laser properly, whereas if tilted on the side, they would appear as thin fibers, visible in bright field, but not reflect the laser enough to appear in laser reflection mode. This highlights that the fibers are formed from stacks of bilayers [38,46], creating ribbons rather than round fibers. To understand the details of the GalC7 fibers inside the GelMA matrix, cryo-scanning electron microscopy (cryo-SEM) was employed.

The supramolecular fibers can be clearly visualized within the GelMA using cryo-SEM (Figs. 4, 5A–E). The fibers display their typical multilayer ribbon-like structures that were also observed in previous work, with similar fiber dimensions that can reach several micrometers in width and around 150 nm in thickness. [38] The characteristic honeycomb structure of GelMA can also be observed surrounding the supramolecular fibers (GelMA control in Fig. 5G–H), similar to what has been reported for GelMA in literature [7,47].

When the gels were swollen in PBS prior to SEM imaging, no fibers were observed (Fig. 5F). To confirm and understand this observation, the stability of the fibers over time was investigated in more detail.

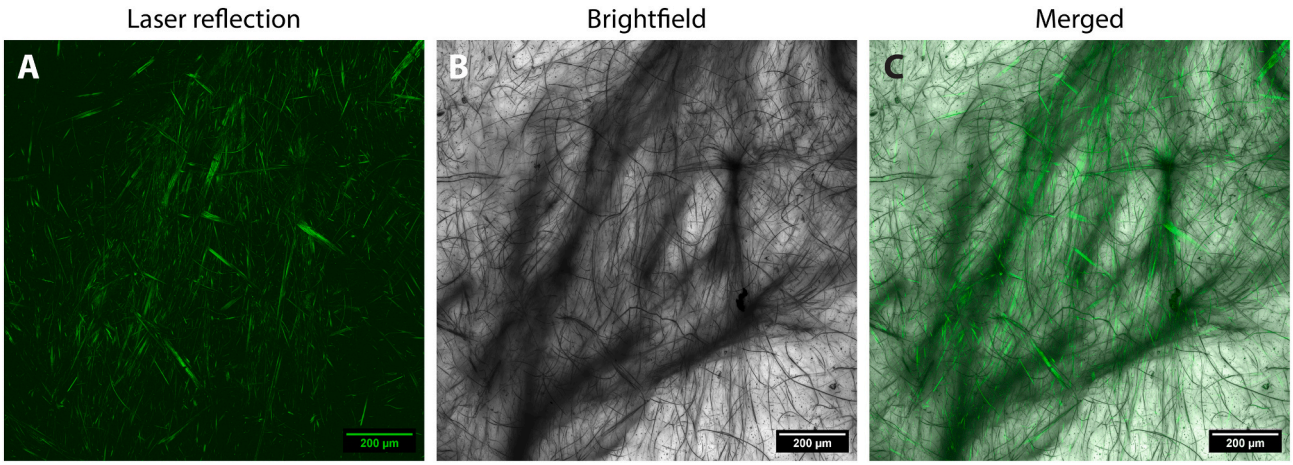

Fig. 4. Confocal microscopy images of the composite gels. Laser reflection (A), bright field (B) and merged (C) images of a composite gel in confocal microscopy (scale bar: 200 μm). All three images are projections of the stacks over a slice of 273 μm.

3.2. Stability of the fiber network in the GelMA matrix

The stability of the GalC7 fibers in the GelMA matrix was quantitatively assessed with brightfield microscopy by imaging composite samples soaking in liquid over time. Time-lapse pictures of a 10 μl composite gel soaking in 1 ml of PBS (containing 0.02 wt% of sodium azide to avoid bacterial degradation of GelMA) were recorded. Fig. 6A shows images of a gel over 3 h. It is clear from the image that the contrast changes markedly over time. We interpret the faint tracks of fibers that remain at 3 h as channels within the GelMA matrix, left after the fibers dissolved.

Image analysis was performed with ImageJ to quantify fiber density over time, which is reported in Fig. 6B. Here, black pixels denote fibers, and each image has been normalized so that we can follow the disappearance of fibers over time (more details in the Experimental section). For composite gels soaking in 1 ml of PBS, the disappearance of the fibers occurs very quickly (Fig. 6B, green), and is indeed complete after 3 h. This result confirms the observation that was made in cryo-SEM, where no remaining supramolecular fibers could be observed in the swollen composite gels. Such dynamic materials may be interesting to mimic tissue remodeling or matrix degradation [35], but it would be ideal to achieve control over the rate of fiber dissolution.

As the fibers are self-assembled from amphiphilic molecules, they are held together by non-covalent interactions. There is equilibrium between the molecules included within the self-assembled fibers and the free molecules in solution. Both the kinetics and the thermodynamics of this equilibrium depend on the molecular structure of the gelator and the external conditions. [39,46] In some systems, this equilibrium is at the origin of reorganization of the self-assembled structures. Also, if the gel is soaked in an external solution, the thermodynamics will drive the system until it reaches the solubility equilibrium.

It is therefore reasonable to assume that the fiber dissolution seen is due to the fact that the system is progressively reaching the solubility equilibrium of GalC7 in the solution used. Previous work has shown that in gels prepared from GalC7 alone in water, the concentration of free GalC7 was 0.03 wt%. [38] When we submerge our gels in PBS, the concentration of free GalC7 will be reduced, a likely driving force for the observed fiber dissolution. If the dissolution is indeed linked to the solubility equilibrium, it should be possible to modulate it by adding free GalC7 to the solution, or by reducing the volume of PBS around the gel. A range of different conditions that alter the dissolution process can be seen in Fig. 6B. In blue, the volume of liquid around the gel is halved. As the fibers begin to dissolve, the GalC7 concentration in solution will increase and act to slow down the dissolution, as evidenced in the measurement. In this case, more than half of the fibers can still be seen after 3 h of soaking, and it took 8 h for the fiber density to go down to 10 %. Similarly, directly dissolving a small amount of GalC7 into the PBS slows down the dissolution. The preparation of the external GalC7/PBS solution is made by dissolving the solid GalC7 into PBS at elevated temperature, followed by cooling to RT. Three concentrations were tested: (0.010; 0.025; and 0.050) wt%.

As can be seen in the graphs in Fig. 6B, the addition of GalC7 to the PBS reduced the fiber degradation rate compared to using PBS only, in a concentration dependent manner. For the highest GalC7 concentration of 0.050 wt%, the fiber density is even seen to increase, as new clusters of fibers formed in the PBS solution. 0.050 wt% is above the equilibrium concentration of GalC7 in water (0.03 wt% [38]) and a fortiori in saline conditions. Thus GalC7 is likely to aggregate in solution, an effect which may have been exacerbated by any liquid evaporation over the time of the experiment, increasing the GalC7 concentration further to initiate self-assembly of the fibers. For lower concentrations of soluble GalC7, below the 0.03 wt% equilibrium concentration, the supramolecular fibers are seen to still degrade over time. 0.025 wt% GalC7 in PBS helped to keep over half of the fibers in the composite gel at 16 h, whereas for 0.010 wt%, the fiber density reached 2 % after 5 h of soaking.

Adding soluble GalC7 to the solution in cell culture poses some specific challenges. The dissolution of the GalC7 solid into liquid requires heating over 100 °C in a sealed vial, which is not compatible with serum containing cell culture media. To still include some GalC7 in the cell culture medium with minimal effect on its composition, the media can be diluted with 10 vol% of a 0.1 wt% solution of GalC7 in PBS and combined with using a minimal volume of media around the gels to extend the time that the fibers are present.

3.2.1. Mechanical properties of the composite gels

We hypothesized that the incorporation of the fibrous network into the GelMA matrix would lead to different mechanical properties of the composite gels compared to pure GelMA. While gels from GalC7 alone were found to be relatively soft in previous work (~15 kPa, measured by compressive test [38]), the individual fibers have a high persistence length and might be assumed to reinforce the gel. To verify this, the mechanical properties of the composite hydrogels were measured with different techniques.

First, force indentation with Atomic Force Microscopy (AFM) was used to probe the gels at the nano-microscale. Several force indentation maps (20 μm × 20 μm or 50 μm × 50 μm) were recorded at separate locations of composite and GelMA gels and analyzed to extract the average Young's modulus of each sample. The results presented in Fig. S3, showed that, overall, the composite hydrogels did not show any difference in Young's modulus compared to pure GelMA. This is likely due to the small indentation depth in AFM (200 nm in our

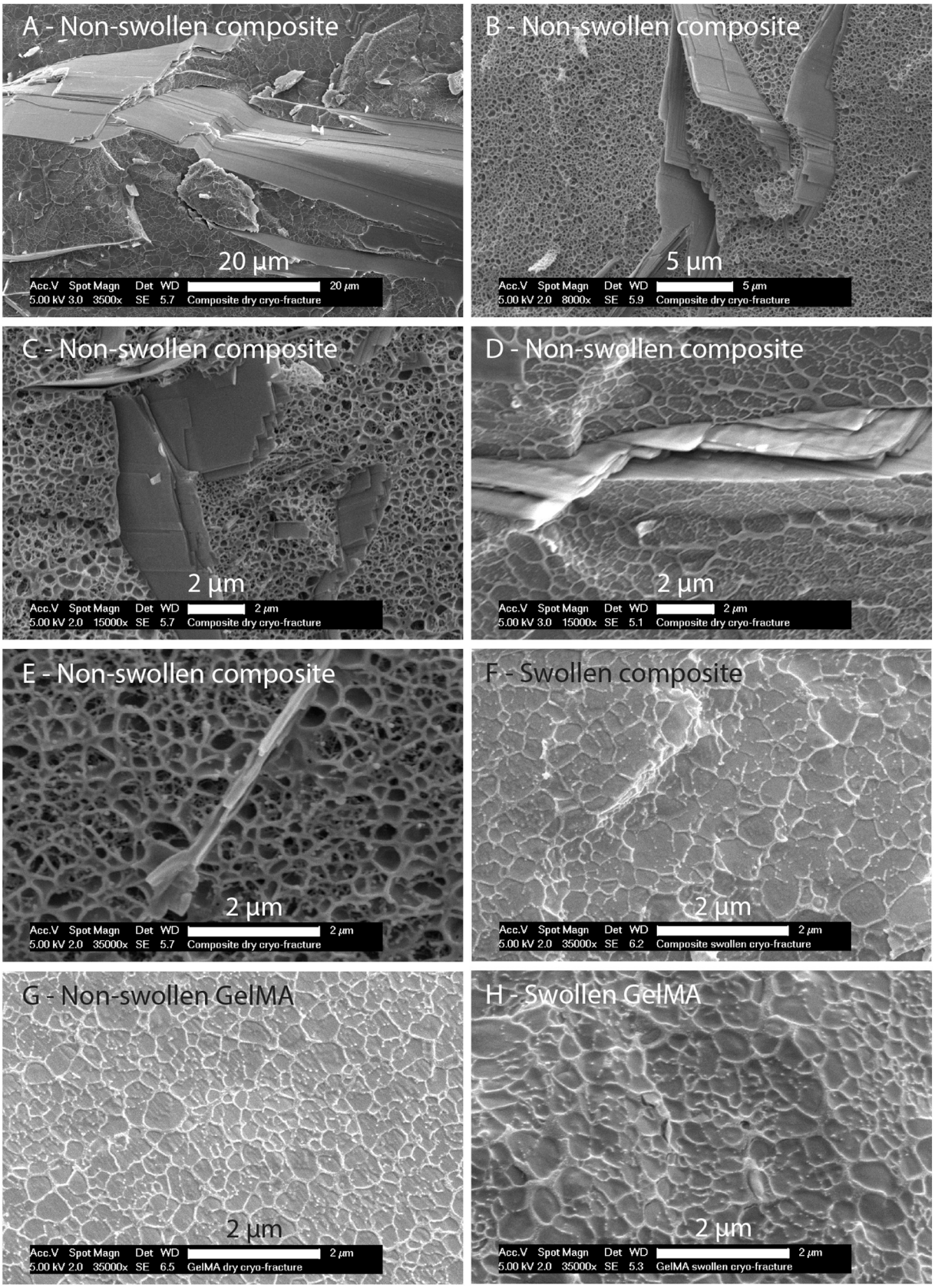

Fig. 5. Cryo-SEM observations of non-swollen composite gel (A–E), swollen composite gel (F), non-swollen pure GelMA (G) and swollen pure GelMA gel (H) at different magnifications (scale bars: A. 20 µm, B. 5 µm, C–H. 2 µm).

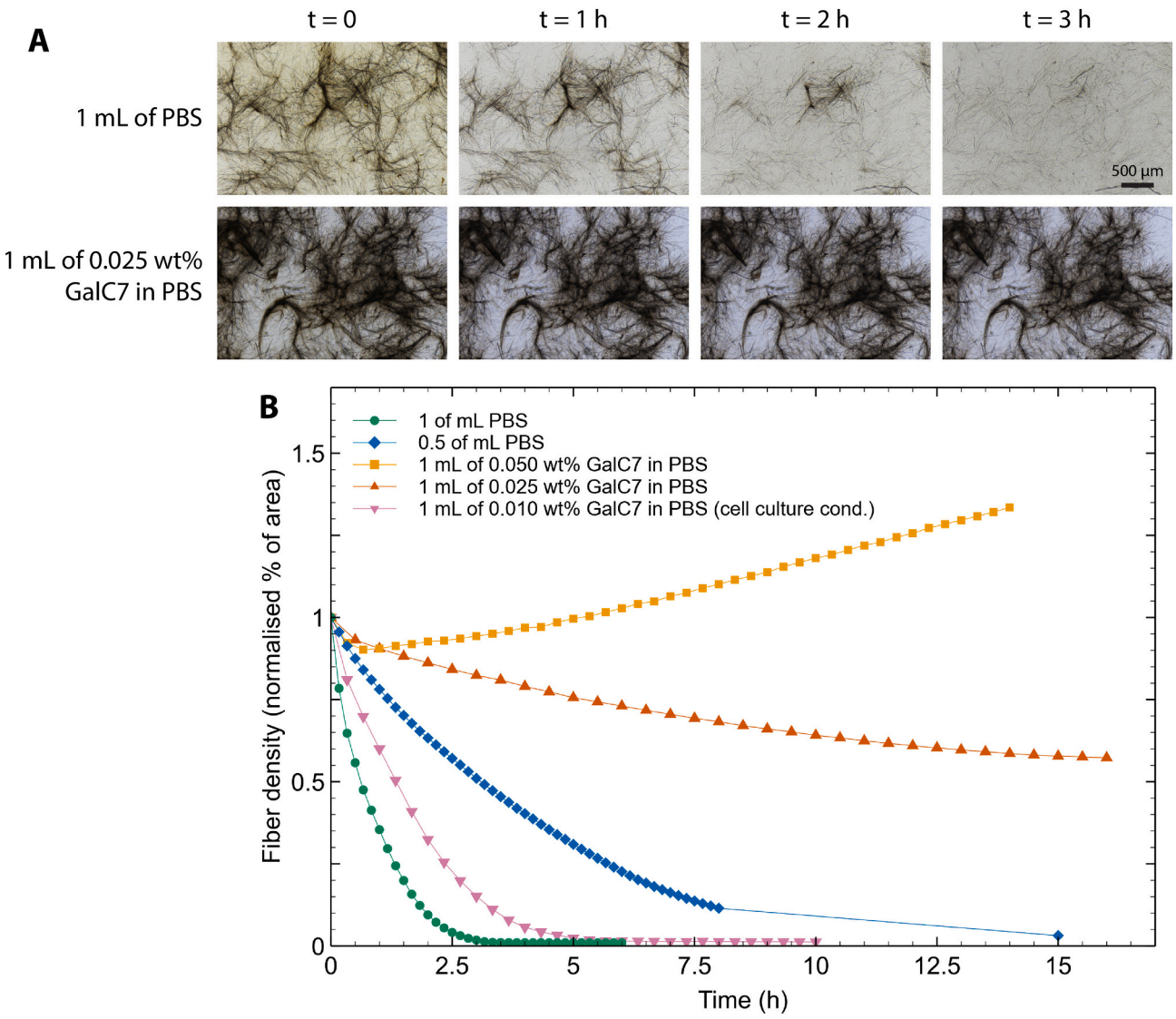

Fig. 6. Quantification of fiber degradation inside the composite gels when soaked in liquid. A) Time-lapse images of two composite hydrogels kept in either PBS or a 0.025 wt% solution of GalC7 in PBS, showing the degradation of the supramolecular fibers over time (scale bar: 500 µm). B) Graph showing the fiber degradation over time by assessing the fiber density on time-lapse microscopy pictures of composite gels in different conditions.

measurements), probing the mechanical properties of the surrounding GelMA, rather than the bulk mechanical properties of the composite gel.

Subsequently, compressive tests were performed on larger composite gels and pure GelMA. Two conditions were tested, directly after cross-linking the samples (referred to as "fresh gels"), and after being swollen in 2 ml of PBS overnight (referred to as "swollen gels") (Fig. 7E and F). Since these gels have a larger volume compared to the ones used in Fig. 6, the fibers are not completely dissolved after one night in PBS, as can be seen in Fig. 7F. Many fibers are seen to remain in the center of the gel. However, many of them have been removed at the outer edges of the disk, which appear less dense. The strain-stress curves generated during the compressive tests on each type of sample can be seen in Fig. 7A and B, whereas Fig. 7C and D show a zoom over the (0−10) % strain range. The Young's modulus of each gel has been determined by applying a linear fit to the (0–10) % strain range and extracting the slope. For both conditions, fresh or swollen gels, the composite hydrogels showed a higher Young's modulus than the pure GelMA gels, with moduli of 81 kPa and 65 kPa for fresh composites compared to 31 kPa and 26 kPa for fresh GelMA, and 40 kPa and 32 kPa for swollen composites against 26 kPa and 24 kPa for swollen GelMA. The partial degradation of the fibrous network is thus confirmed by the approximately 50 % decrease in Young's modulus after swelling the composite gels, whereas the decrease for the swollen compared to fresh GelMA alone was only approximately 12 %, which could be due to the loosened polymer network after swelling. This is in agreement with previous literature on GelMA of similar composition, and with the same photoinitiator system, with the resulting modulus depending on polymer concentration, photoinitiator concentration and light irradiation. [10,12]

Stress-strain curves also display differences between the gels in terms of stress at failure. For instance, the fresh composite gels failed at a much lower stress than the fresh GelMA gels (~150 kPa for composite compared to ~420 kPa for GelMA, Fig. 7A). This could be explained by the presence of the fibers inside the GelMA matrix that might act as stress concentrators where fracture can nucleate, whereas the pure GelMA gels have a more homogeneous structure and, evidently, can sustain a higher stress. When the gels are swollen, and the fibers partially degraded, (Fig. 7B), both composite and pure GelMA gels fail at approximately 230 kPa.

To further investigate the macroscopic mechanical properties of the composite hydrogels, tensile testing was also employed. This mode of mechanical testing is particularly relevant in the case of materials used for tissue engineering applications where the tissue needs to be

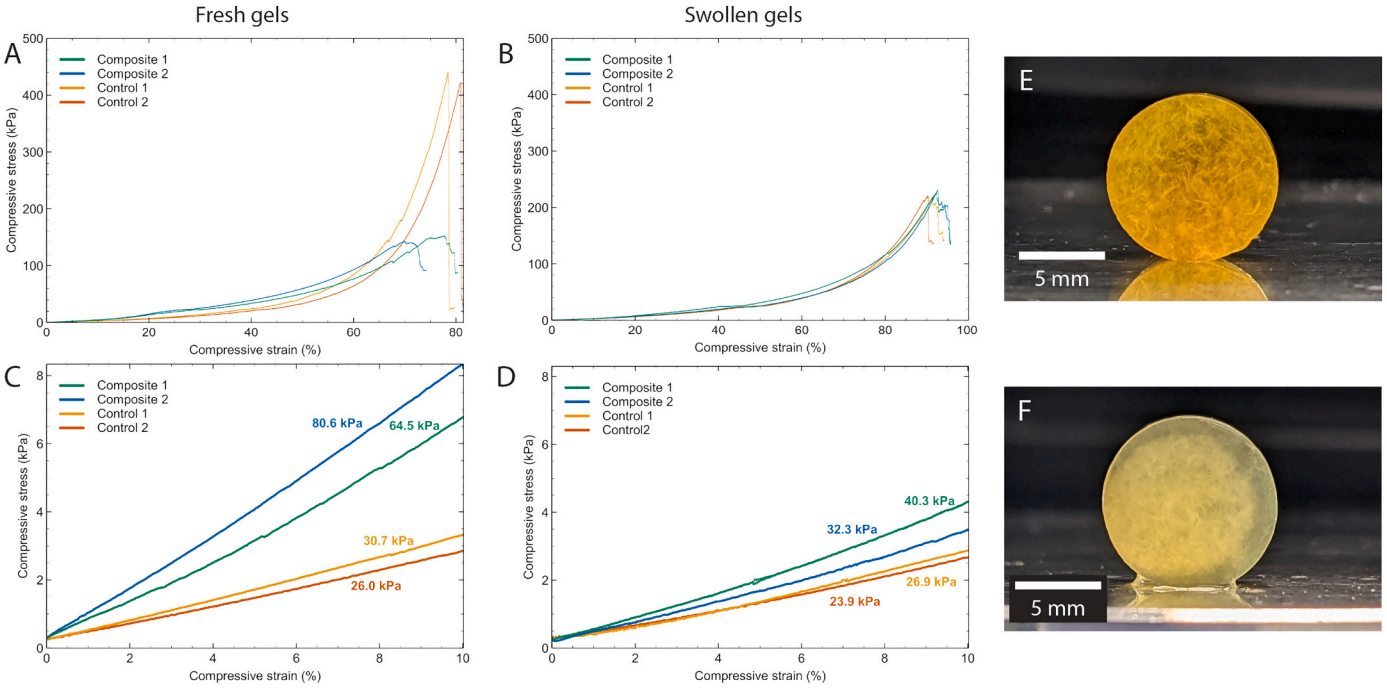

Fig. 7. Results of compressive tests on fresh (A, C) and swollen (B, D) composite gels and controls of pure GelMA (strain rate: 1 mm/min). A and B show the whole stress-strain curves until failure, whereas C and D show a zoom over the (0–10) % compressive strain region. For each gel, the Young's modulus was estimated by applying a linear fit to the (0–10) % compressive strain range and extracting the slope. Pictures of fresh (E) and swollen (F) composite gels before the tests (scale bar: 5 mm).

mechanically loaded (either through external stimulus, or via cell contractions, such as in cardiac tissue engineering). [48] Dog bone samples of composite gels and controls of pure GelMA gels were prepared and tested on a custom-built mechanical testing device that allowed samples to be stretched and released at a controlled strain rate while measuring the force exerted on the sample. [49] The results of these tests are presented in Fig. 8.

Tensile tests were performed while the samples were soaking in PBS (thus in swollen state), and after a first stretch until 20 % strain, cyclic tensile testing of the gels was performed at 0.1 mm/s until 20 % strain, three times. The curves in Fig. 8A show the first cycle. The curves for the composite hydrogels show a higher slope compared to the GelMA controls, equating to a higher Young's modulus. The difference seen in the Young's modulus between the composite replicates might be due to differences in fiber density inside the gel, because of pre-gel solution preparation and/or any difference in time that the gels have been in a liquid environment, as that leads to fiber degradation.

Interestingly, the composite gels display a hysteresis in the tensile load and unload curves, significantly larger than the pure GelMA, which is characteristic of energy dissipation, probably due to the presence of fibers. This may be due to slip between the fibers, or within the fibers themselves, or due to slip or unbinding of hydrogen bonds between the fibers and the GelMA. This energy dissipation tendency has been quantified also by rheology in earlier work, giving a loss modulus G" of 1 kPa for a storage modulus G' of 7 kPa in the pure GalC7 gels. [38] Many different strategies have been employed in literature to design hydrogels with large energy dissipation [50], including double network gels [51–54] and nanocomposite gels [55,56].

To characterize the variation of elastic modulus with fiber degradation (Fig. 8B), tensile tests were also performed over time for composite gels and pure GelMA controls. Over the course of 2 h, the GelMA control gels can be observed to have relatively stable tensile Young's modulus. Both controls display a moderate increase in the modulus, with 2 kPa higher modulus after 2 h. This is surprising, as gel swelling generally is associated with a reduction of Young's modulus. [57] However, the modulus of a polymer gel can be assumed to be proportional to the chain number density and the elastic free energy per chain, of which the elastic energy per chain increases during swelling, while the chain number density decreases. [58] Therefore predictions of the influence of hydrogel swelling on the modulus are challenging even in simple gel systems [57], and even more so for composite gels such as the ones presented in this work. The data suggest however, that there is a significant increase in elastic energy in the system as swelling is initiated, resulting in the observed increase in Young's modulus.

As expected, there was no effect on the Young's modulus by adding GalC7 to the solution surrounding the GelMA control gel. For the composite gels, an initial increase in the modulus during the first 30 min was replaced by a decrease of the modulus, if there is no GalC7 in the solution. This can be attributed to the dissolution of the fibers, with Young's modulus of the composite gel decreasing to be similar to GelMA alone. As seen previously, the addition of GalC7 in solution prevented the fiber dissolution within the timeframe tested here, manifesting as a continued slight increase in the Young's modulus, possibly due to swelling, and potentially contributed to any initiation of new fiber growth.

3.3. Culture of cardiac fibroblasts

While the dissolution of the fibers occurred faster than we had expected, we were interested to culture cells inside the composite hydrogels to confirm that they are suitable for cell culture, and to see if cells were able to interact with the channels left in the gel after the supramolecular fibers dissolve. To this end, we embedded cardiac fibroblasts in the composite and GelMA control gels and evaluated the experiment after 6 h or 7 days in culture. The conditions of the cell culture were tailored to reduce the fiber dissolution, but were limited by the inability to heat the cell culture media to 100 °C. Consequently, 0.01 wt% of GalC7 was added to the media that surrounded the gels, and the volume of media was kept at 0.5 ml. With these conditions, at least some fibers should remain at 6 h, our early time point. At 7 days, all fibers are

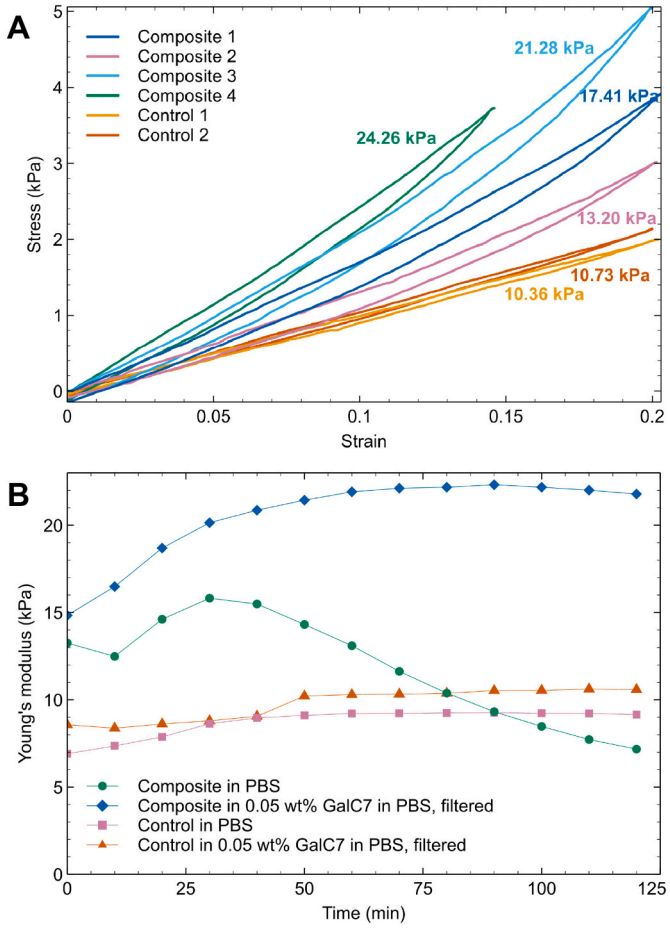

Fig. 8. A) Tensile test results on composite and control (pure GelMA) gels. Four replicates of the composite have been measured. For each sample, the graph shows the first of three strain cycles up to 20 % at a rate of 0.1 mm/s. Measurements were all performed in PBS. The Young's moduli were calculated by applying a linear fit to the (load) stress-strain curve and extracting the slope. B) Young's moduli of composite and pure GelMA gels over time when soaking in either PBS or a solution of 0.05 wt% of GalC7 in PBS.

anticipated to have dissolved, and been replaced by cavities in the GelMA. Representative images from the cell culture can be seen in Fig. 9, with more images available in supporting information Fig. S4 (6 h) and Fig. S5 (7 days).

Live/dead staining after 7 days in culture (Fig. 9A–C) showed excellent viability, with very few dead (red) cells seen. The morphology of the cells is more easily visualized by immunostaining of the actin cytoskeleton using phalloidin (and the nucleus is stained blue using DAPI). After 6 h of culture, most cells remain round in both the GelMA control and the composite gels. Some cells, however, are seen to extend in an elongated morphology in the composite gels. As the fibers are expected to have been present over this initial period, we interpret this as the cells being able to interact with and extend along the fibers. This is in agreement with previous work where neural stem cells, grown in pure GalC7 gels for 7 days, displayed long and straight neurite extensions when they differentiated as neurons. [38] Cells are also known to extend along fibers in the ECM in vivo as well as in vitro. For example, cells have been demonstrated to extend along topographical cues in 2D, when ridges/grooves [59,60] or protein patterns [61,62] are presented on the micrometer or nanometer scale [63]. Such topographical guidance has also been demonstrated in 3D, in several composite hydrogel systems. [4,24,64,65] Other interesting composite gels, that have demonstrated cell guidance through alignment, include those with freezing-induced aligned porosity, such as in work on GelMA/Silk fibroin scaffolds by Asuncion et al. [66] With a strategy close to our, the culture of fibroblasts in a GelMA hydrogel with embedded sacrificial polyvinylalcohol (PVA) fibers led to a directional growth of the cells. In this case, the microchannels (around 50 μm) are larger than the channels formed in our work (3–4 μm, measured from the width of the cell extensions) and smaller than those made by microfabrication techniques (≈500 μm). [67] These small diameters are interesting for mimicking microvascularization.

After 7 days in culture, cells can be seen to extend more within the GelMA controls, and this can be attributed to degradation of GelMA by the cells creating space for the cells to extend. Cells can be seen to both extend in several directions, or in some cases to create elongated cells similar to those in the composite gels. In the composite gels, more cells are elongated and of very high aspect ratio. These elongated cells are remarkably narrow, and cells do not appear to spread in all directions as seen in the GelMA. Also, examples of chains of single cells can be seen, demonstrated by several nuclei observed along them. We interpret this as the cells interacting with the cavities left in the gel after the fibers have dissolved, most likely squeezing through the narrow channels, and following, it seems, the path of least resistance. The fact that the degraded fibers leave space in the hydrogel is interesting for several reasons. This outcome will increase porosity and thus permeation of oxygen and nutrients into the scaffold over time as cells proliferate. [68,69] In the PVA-GelMA composites by Sun et al., the channels were larger and accommodated the growth of several cells in their width. [67] Many challenges remain to fully understand how cells interact with their surroundings in 3D. A particular challenge is that several factors are generally coupled in hydrogel systems, such as porosity and modulus, and these gels offer an unprecedented opportunity to independently tailor porosity and gel modulus. For this reason, we believe that these gels will be of interest to study many biological processes, and in particular vascularization [70,71], and cancer metastasis and invasion. [20] In addition, these gels present dynamic mechanical properties, which we believe can be further tailored to suit various applications using GalC7 in solution, or perhaps by tuning the fiber composition using mixes of other *N*-alkyl-galactonamide molecules. [38,72]

4. Conclusion

In summary, we developed a novel composite hydrogel comprising supramolecular fibers from small self-assembling synthetic molecules inside a modified gelatin matrix. By directly mixing GelMA and GalC7 in PBS at high temperature followed by a slow cooling, we managed to incorporate a homogeneous fibrous network of GalC7 fibers inside a GelMA hydrogel, as characterized through several microscopy techniques. Our results showed that the fibers inside the GelMA disappear over time due to the non-covalent nature of the interactions governing the GalC7 fibers, which ultimately results in their dissolution. However, the rate of this degradation can be tuned by using smaller liquid volumes and/or a small concentration of GalC7 dissolved in the surrounding liquid in which the composite gels are kept. Our results also showed that the presence of the supramolecular fibers inside the GelMA matrix increases the constructs' stiffness compared to GelMA alone. As a result of fiber dissolution, narrow channels develop in the GelMA matrix, along with a gradual softening of the gel. Finally, we successfully encapsulated and cultured cardiac fibroblast cells for 7 days inside the composite gels. Our results showed that the composite gels enabled remarkable elongation of fibroblasts in 3D, which was not observed inside pure GelMA gels. This novel composite material thus brings particularly interesting properties to the resulting scaffolds for their use in tissue engineering applications. The presence of the supramolecular fibers as well as their degradation over time provides a dynamic environment for cell culture with evolving mechanical properties and enhanced porosity. We believe that there is potential for the use of such materials in scar tissue or vascularization studies where changes in cell microenvironment are key factors for understanding such mechanisms.

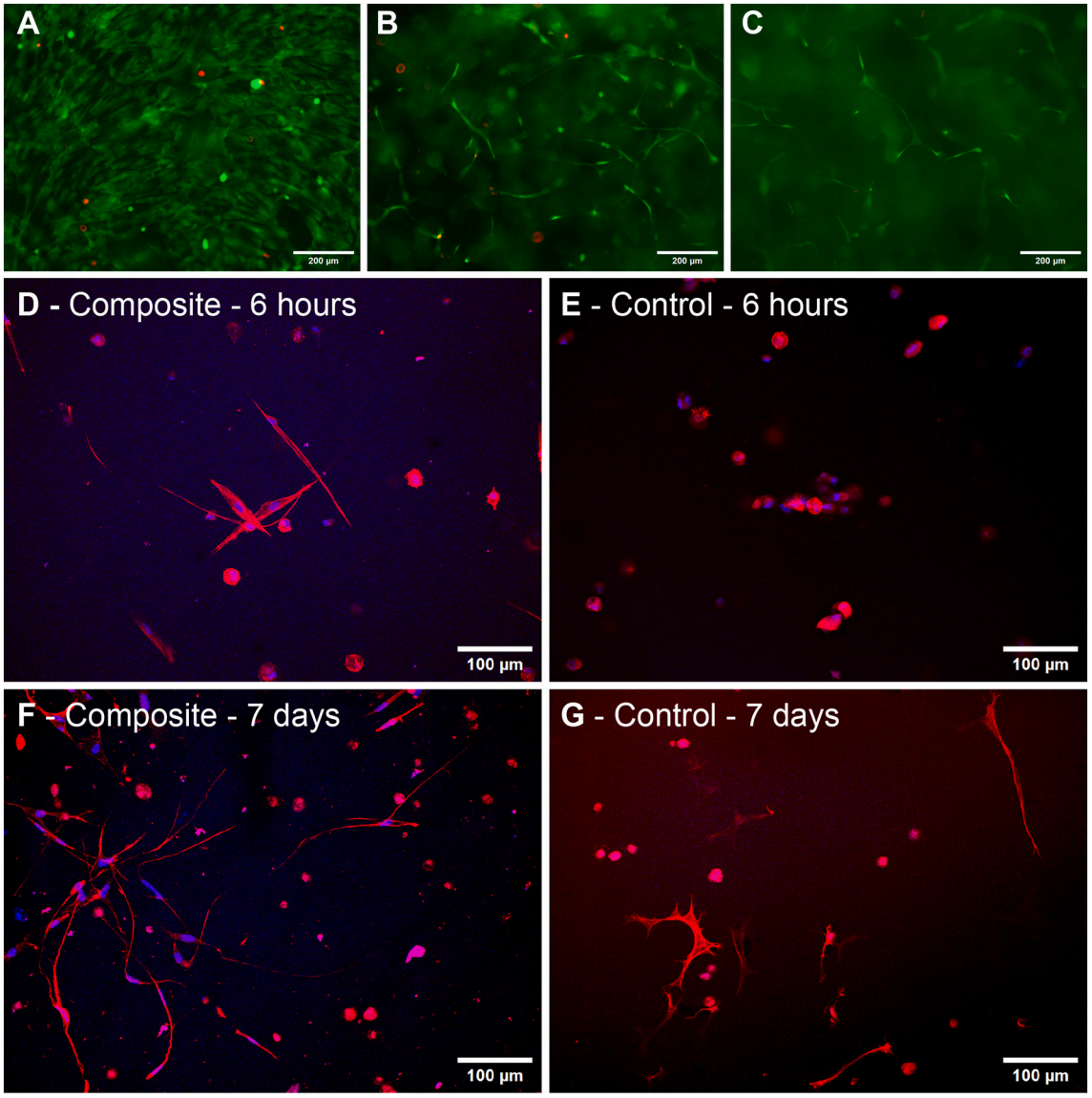

Fig. 9. Biocompatibility assay on the composite gels showing the live (green)/dead (red) staining of cardiac fibroblasts after 7 days of culture encapsulated in composite gels (A–C, scale bar: 200 µm).Immunostaining of cardiac fibroblasts encapsulated in composite hydrogels (D,F) and GelMA controls (E, G) after 6 h and 7 days in culture (blue: DAPI, red: phalloidin, scale bar: 100 µm).

Funding sources

Financial support is acknowledged from the Faculty of Engineering of the University of Auckland (Faculty Research and Development Fund), the MacDiarmid Institute for Advanced Materials and Nanotechnology, the Health Research Council of New Zealand, and the James Cook Research Fellowship and Rutherford Discovery Fellowship, from Government funding, managed by Royal Society Te Apārangi.

CRediT authorship contribution statement

Anaïs E. Chalard: Writing – original draft, Supervision, Methodology, Formal analysis, Data curation, Conceptualization. **Harrison Porritt:** Writing – review & editing, Investigation, Data curation. **Emily J. Lam Po Tang:** Writing – review & editing, Methodology, Data curation. **Andrew J. Taberner:** Writing – review & editing, Supervision, Methodology. **Annika Winbo:** Writing – review & editing, Supervision, Resources, Methodology, Data curation. **Amatul M. Ahmad:** Writing – review & editing, Methodology, Data curation. **Juliette Fitremann:** Writing – review & editing, Conceptualization. **Jenny Malmström:** Writing – review & editing, Supervision, Resources, Funding acquisition, Conceptualization.

Declaration of competing interest

The authors declare the following financial interests/personal relationships which may be considered as potential competing interests: J. Fitremann can receive royalties from the selling of N-heptyl-D-galactonamide by the company Innov'Orga (France). These royalties expected would represent very low amounts and in any case they will not influence her scientific statements related to with this molecule. J. Malmström is an associate editor of Biomaterials Advances. If there are other authors, they declare that they have no known competing financial interests or personal relationships that could have appeared to influence the work reported in this paper.

Data availability

Data will be made available on request.

Acknowledgements

The authors thank A/Prof Khoon Lim for supplying chemicals and for his advice, Eda Vella for their help with the use of the AFM, and Prof Johanna Montgomery for letting us use her cell culture facilities. The authors would also like to thank Jacqueline Ross for assistance with the confocal microscopy and Catherine Hobbis for the help with cryo-SEM.

Appendix A. Supplementary data

A PDF file containing supplementary figures is available online free of charge. It contains mechanical measurements of GelMA after exposure to high temperature, the cooling ramp used for the supra-molecular self-assembly, Atomic Force Microscopy force indentation data for composite gels and additional images of cardiac fibroblasts cultured in the composite GelMA and pure GelMA. Supplementary data to this article can be found online at https://doi.org/10.1016/j.bioadv.2024.213957.

References

[1] S. Hinderer, S.L. Layland, K. Schenke-Layland, ECM and ECM-like materials — biomaterials for applications in regenerative medicine and cancer therapy, Adv. Drug Deliv. Rev. 97 (Feb. 2016) 260–269, https://doi.org/10.1016/j.addr.2015.11.019.

[2] Y. Xing, B. Varghese, Z. Ling, A.S. Kar, E. Reinoso Jacome, X. Ren, Extracellular matrix by design: native biomaterial fabrication and functionalization to boost tissue regeneration, Regener. Eng. Transl. Med. 8 (1) (Mar. 2022) 55–74, https://doi.org/10.1007/s40883-021-00210-5.

[3] J.C. Valdoz, et al., The ECM: to scaffold, or not to scaffold, that is the question, Int. J. Mol. Sci. 22 (23) (2021), https://doi.org/10.3390/ijms222312690.

[4] S.K. Asl, M. Rahimzadegan, A.K. Asl, Progress in cardiac tissue engineering and regeneration: implications of gelatin-based hybrid scaffolds, Int. J. Biol. Macromol. 261 (Mar. 2024) 129924, https://doi.org/10.1016/j.ijbiomac.2024.129924.

[5] B.N. Narasimhan, M.S. Horrocks, J. Malmström, Hydrogels with tunable physical cues and their emerging roles in studies of cellular mechanotransduction, Adv. NanoBiomed. Res. 1 (10) (2021) 2100059, https://doi.org/10.1002/anbr.202100059.

[6] A. Guo, S. Zhang, R. Yang, C. Sui, Enhancing the mechanical strength of 3D printed GelMA for soft tissue engineering applications, Mater. Today Bio. 24 (2024), https://doi.org/10.1016/j.mtbio.2023.100939.

[7] K. Yue, G. Trujillo-de Santiago, M.M. Alvarez, A. Tamayol, N. Annabi, A. Khademhosseini, Synthesis, properties, and biomedical applications of gelatin methacryloyl (GelMA) hydrogels, Biomaterials 73 (Dec. 2015) 254–271, https://doi.org/10.1016/j.biomaterials.2015.08.045.

[8] M. Sun, X. Sun, Z. Wang, S. Guo, G. Yu, H. Yang, Synthesis and properties of gelatin methacryloyl (GelMA) hydrogels and their recent applications in load-bearing tissue, Polymers 10 (11) (2018), https://doi.org/10.3390/POLYM10111290.

[9] D. Loessner, et al., Functionalization, preparation and use of cell-laden gelatin methacryloyl–based hydrogels as modular tissue culture platforms, Nat. Protoc. 11 (4) (Apr. 2016) 727–746, https://doi.org/10.1038/nprot.2016.037.

[10] K.S. Lim, et al., Visible light cross-linking of gelatin hydrogels offers an enhanced cell microenvironment with improved light penetration depth, Macromol. Biosci. 19 (6) (2019) 1900098, https://doi.org/10.1002/mabi.201900098.

[11] N. Monteiro, et al., Photopolymerization of cell-laden gelatin methacryloyl hydrogels using a dental curing light for regenerative dentistry, Dent. Mater. 34 (3) (Mar. 2018) 389–399, https://doi.org/10.1016/j.dental.2017.11.020.

[12] A.E. Chalard, A.W. Dixon, A.J. Taberner, J. Malmström, Visible-light stiffness patterning of GelMA hydrogels towards in vitro scar tissue models, Front.Cell Dev. Biol. 10 (May 2022), https://doi.org/10.3389/fcell.2022.946754.

[13] I. Noshadi, et al., In vitro and in vivo analysis of visible light crosslinkable gelatin methacryloyl (GelMA) hydrogels, Biomater. Sci. 5 (10) (2017) 2093–2105, https://doi.org/10.1039/C7BM00110J.

[14] K.S. Lim, et al., New visible-light photoinitiating system for improved print fidelity in gelatin-based bioinks, ACS Biomater. Sci. Eng. 2 (10) (Oct. 2016) 1752–1762, https://doi.org/10.1021/acsbiomaterials.6b00149.

[15] M.D. Davidson, J.A. Burdick, R.G. Wells, Engineered biomaterial platforms to study fibrosis, Adv. Healthc. Mater. 9 (8) (Apr. 2020) 1901682, https://doi.org/10.1002/adhm.201901682.

[16] K. Sun, X. Li, P.E. Scherer, Extracellular matrix (ECM) and fibrosis in adipose tissue: overview and perspectives, in: Y.S. Prakash (Ed.), Comprehensive Physiology, 1st ed, Wiley, 2023, pp. 4387–4407, https://doi.org/10.1002/cphy.c220020.

[17] N.R. Ariyasinghe, D.M. Lyra-Leite, M.L. McCain, Engineering cardiac microphysiological systems to model pathological extracellular matrix remodeling, Am. J. Phys. Heart Circ. Phys. 315 (4) (Oct. 2018) H771–H789, https://doi.org/10.1152/ajpheart.00110.2018.

[18] J.M. Shapiro, M.L. Oyen, Hydrogel composite materials for tissue engineering scaffolds, JOM 65 (4) (Apr. 2013) 505–516, https://doi.org/10.1007/s11837-013-0575-6.

[19] C. Sheffield, K. Meyers, E. Johnson, R. Rajachar, Application of composite hydrogels to control physical properties in tissue engineering and regenerative medicine, Gels 4 (2) (May 2018) 51, https://doi.org/10.3390/gels4020051.

[20] J. Sievers, V. Mahajan, P.B. Welzel, C. Werner, A. Taubenberger, Precision hydrogels for the study of cancer cell mechanobiology, Adv. Healthc. Mater. 12 (14) (Jun. 2023) 2202514, https://doi.org/10.1002/adhm.202202514.

[21] E.S. Lisboa, et al., Nanomaterials-combined methacrylated gelatin hydrogels (GelMA) for cardiac tissue constructs, J. Control. Release 365 (Jan. 2024) 617–639, https://doi.org/10.1016/j.jconrel.2023.11.056.

[22] T.A. Arica, M. Guzelgulgen, A.A. Yildiz, M.M. Demir, Electrospun GelMA fibers and p(HEMA) matrix composite for corneal tissue engineering, Mater. Sci. Eng. C 120 (Jan. 2021) 111720, https://doi.org/10.1016/j.msec.2020.111720.

[23] L.E. Beckett, J.T. Lewis, T.K. Tonge, L.T.J. Korley, Enhancement of the mechanical properties of hydrogels with continuous fibrous reinforcement, ACS Biomater. Sci. Eng. 6 (10) (Oct. 2020) 5453–5473, https://doi.org/10.1021/acsbiomaterials.0c00911.

[24] D.L. Matera, W.Y. Wang, M.R. Smith, A. Shikanov, B.M. Baker, Fiber density modulates cell spreading in 3D interstitial matrix mimetics, ACS Biomater. Sci. Eng. 5 (6) (Jun. 2019) 2965–2975, https://doi.org/10.1021/acsbiomaterials.9b00141.

[25] M. Zhang, et al., Electrospun nanofiber/hydrogel composite materials and their tissue engineering applications, J. Mater. Sci. Technol. 162 (Nov. 2023) 157–178, https://doi.org/10.1016/j.jmst.2023.04.015.

[26] Z. Wei, et al., Fiber microarchitecture in interpenetrating collagen–alginate hydrogel with tunable mechanical plasticity regulates tumor cell migration, Adv. Healthc. Mater. (Aug. 2023) 2301586, https://doi.org/10.1002/adhm.202301586.

[27] Z. Montaseri, S.S. Abolmaali, A.M. Tamaddon, F. Farvadi, Composite silk fibroin hydrogel scaffolds for cartilage tissue regeneration, J. Drug Deliv. Sci. Technol. 79 (Jan. 2023) 104018, https://doi.org/10.1016/j.jddst.2022.104018.

[28] S.J. Buwalda, Bio-based composite hydrogels for biomedical applications, Multifunct. Mater. 3 (2) (May 2020) 022001, https://doi.org/10.1088/2399-7532/ab80d6.

[29] C. Chen, J. Zhou, J. Chen, H. Liu, Advances in DNA supramolecular hydrogels for tissue engineering, Macromol. Biosci. 22 (12) (2022), https://doi.org/10.1002/mabi.202200152.

[30] X. Yan, et al., Advances in the application of supramolecular hydrogels for stem cell delivery and cartilage tissue engineering, Front. Bioeng. Biotechnol. 8 (2020), https://doi.org/10.3389/fbioe.2020.00847.

[31] L. Saunders, P.X. Ma, Self-healing supramolecular hydrogels for tissue engineering applications, Macromol. Biosci. 19 (1) (2019), https://doi.org/10.1002/mabi.201800313.

[32] R. Kubota, Supramolecular–polymer composite hydrogels: from in situ network observation to functional properties, Bull. Chem. Soc. Jpn. 96 (8) (Aug. 2023) 802–812, https://doi.org/10.1246/bcsj.20230129.

[33] N.A. Sather, et al., 3D printing of supramolecular polymer hydrogels with hierarchical structure, Small 17 (5) (Feb. 2021) 2005743, https://doi.org/10.1002/smll.202005743.

[34] D.J. Cornwell, D.K. Smith, Expanding the scope of gels – combining polymers with low-molecular-weight gelators to yield modified self-assembling smart materials with high-tech applications, Mater. Horiz. 2 (3) (2015) 279–293, https://doi.org/10.1039/C4MH00245H.

[35] W. Xie, et al., Static and dynamic: evolving biomaterial mechanical properties to control cellular Mechanotransduction, Adv. Sci. 10 (9) (2023) 2204594, https://doi.org/10.1002/advs.202204594.

[36] F. Netti, M. Aviv, Y. Dan, S. Rudnick-Glick, M. Halperin-Sternfeld, L. Adler-Abramovich, Stabilizing gelatin-based bioinks under physiological conditions by incorporation of ethylene-glycol-conjugated Fmoc-FF peptides, Nanoscale 14 (23) (2022) 8525–8533, https://doi.org/10.1039/D1NR08206J.

[37] M. Maisani, et al., A new composite hydrogel combining the biological properties of collagen with the mechanical properties of a supramolecular scaffold for bone tissue engineering, J. Tissue Eng. Regen. Med. 12 (3) (2018) e1489–e1500, https://doi.org/10.1002/term.2569.

[38] A. Chalard, et al., Simple synthetic molecular hydrogels from self-assembling alkylgalactonamides as scaffold for 3D neuronal cell growth, ACS Appl. Mater. Interfaces 10 (20) (May 2018) 17004–17017, https://doi.org/10.1021/acsami.8b01365.

[39] A. Chalard, et al., Wet spinning and radial self-assembly of a carbohydrate low molecular weight gelator into well organized hydrogel filaments, Nanoscale 11 (32) (2019) 15043–15056, https://doi.org/10.1039/C9NR02727K.

[40] A. Chalard, M. Mauduit, S. Souleille, P. Joseph, L. Malaquin, J. Fitremann, 3D printing of a biocompatible low molecular weight supramolecular hydrogel by dimethylsulfoxide water solvent exchange, Addit. Manuf. 33 (May 2020) 101162, https://doi.org/10.1016/j.addma.2020.101162.

[41] J.M. Zatorski, A.N. Montalbine, J.E. Ortiz-Cárdenas, R.R. Pompano, Quantification of fractional and absolute functionalization of gelatin hydrogels by optimized ninhydrin assay and 1H NMR, Anal. Bioanal. Chem. 412 (24) (Sep. 2020) 6211–6220, https://doi.org/10.1007/s00216-020-02792-5.

[42] H. Schillers, et al., Standardized Nanomechanical atomic force microscopy procedure (SNAP) for measuring soft and biological samples, Sci. Rep. 7 (1) (Dec. 2017) 5117, https://doi.org/10.1038/s41598-017-05383-0.

[43] H.R. Hertz, Über die Berührung fester elastischer Körper und über die Härte, in: Verhandlungen des Vereins zur Beförderung des Gewerbefleißes 1882, Berlin : Verein zur Beförderung des Gewerbefleisses, 1882, pp. 449–463.

[44] T.R. Matzelle, G. Geuskens, N. Kruse, Elastic properties of poly(*N*-isopropylacrylamide) and poly(acrylamide) hydrogels studied by scanning force

microscopy, Macromolecules 36 (8) (Apr. 2003) 2926–2931, https://doi.org/10.1021/ma021719p.
[45] G.N. Greaves, A.L. Greer, R.S. Lakes, T. Rouxel, Poisson's ratio and modern materials, Nat. Mater. 10 (11) (Nov. 2011) 823–837, https://doi.org/10.1038/nmat3134.
[46] M.J. Clemente, P. Romero, J.L. Serrano, J. Fitremann, L. Oriol, Supramolecular hydrogels based on Glycoamphiphiles: effect of the disaccharide polar head, Chem. Mater. 24 (20) (Oct. 2012) 3847–3858, https://doi.org/10.1021/cm301509v.
[47] C. Kim, et al., Stem cell Mechanosensation on gelatin Methacryloyl (GelMA) stiffness gradient hydrogels, Ann. Biomed. Eng. 48 (2) (Feb. 2020) 893–902, https://doi.org/10.1007/s10439-019-02428-5.
[48] J.M. Bliley, et al., Dynamic loading of human engineered heart tissue enhances contractile function and drives a desmosome-linked disease phenotype, Sci. Transl. Med. (Jul. 2021), https://doi.org/10.1126/scitranslmed.abd1817.
[49] A. Taberner, et al., A dynamometer for nature's engines, IEEE Instrum. Meas. Mag. 22 (2) (Apr. 2019) 10–16, https://doi.org/10.1109/MIM.2019.8674628.
[50] M. Li, Y. Lin, Y. Zhang, L. Bian, K. Zhang, Energy-dissipative hydrogels: a promising material for tissue regeneration†, Chin. J. Chem. 41 (20) (2023) 2697–2714, https://doi.org/10.1002/cjoc.202300167.
[51] B.N. Narasimhan, G.S. Deijs, S. Manuguri, M.S.H. Ting, M.A.K. Williams, J. Malmström, A comparative study of tough hydrogen bonding dissipating hydrogels made with different network structures, Nanoscale Adv. 3 (10) (2021) 2934–2947, https://doi.org/10.1039/D1NA00103E.
[52] B.N. Narasimhan, A.W. Dixon, B. Mansel, A. Taberner, J. Mata, J. Malmström, Hydrogen bonding dissipating hydrogels: the influence of network structure design on structure–property relationships, J. Colloid Interface Sci. 630 (Jan. 2023) 638–653, https://doi.org/10.1016/j.jcis.2022.10.029.
[53] C. Creton, 50th anniversary perspective: networks and gels: soft but dynamic and tough, Macromolecules 50 (21) (Nov. 2017) 8297–8316, https://doi.org/10.1021/acs.macromol.7b01698.
[54] W. Zhang, et al., Double-network hydrogels for biomaterials: structure-property relationships and drug delivery, Eur. Polym. J. 185 (Feb. 2023) 111807, https://doi.org/10.1016/j.eurpolymj.2022.111807.
[55] F. Cheng, H. Chen, H. Li, Recent advances in tough and self-healing nanocomposite hydrogels for shape morphing and soft actuators, Eur. Polym. J. 124 (Feb. 2020) 109448, https://doi.org/10.1016/j.eurpolymj.2019.109448.
[56] Y. Zhang, Q. Chen, Z. Dai, Y. Dai, F. Xia, X. Zhang, Nanocomposite adhesive hydrogels: from design to application, J. Mater. Chem. B 9 (3) (Jan. 2021) 585–593, https://doi.org/10.1039/D0TB02000A.
[57] R. Subramani, et al., The influence of swelling on elastic properties of polyacrylamide hydrogels, Front. Mater. 7 (Jul. 2020) 212, https://doi.org/10.3389/fmats.2020.00212.
[58] Z. Li, Z. Liu, T.Y. Ng, P. Sharma, The effect of water content on the elastic modulus and fracture energy of hydrogel, Extreme Mech. Lett. 35 (Feb. 2020) 100617, https://doi.org/10.1016/j.eml.2019.100617.
[59] A. Béduer, C. Vieu, F. Arnauduc, J.-C. Sol, I. Loubinoux, L. Vaysse, Engineering of adult human neural stem cells differentiation through surface micropatterning, Biomaterials 33 (2) (Jan. 2012) 504–514, https://doi.org/10.1016/j.biomaterials.2011.09.073.
[60] S. Al-Haque, et al., Hydrogel substrate stiffness and topography interact to induce contact guidance in cardiac fibroblasts, Macromol. Biosci. 12 (10) (2012) 1342–1353, https://doi.org/10.1002/mabi.201200042.
[61] P. Camelliti, A.D. McCulloch, P. Kohl, Microstructured cocultures of cardiac myocytes and fibroblasts: a two-dimensional in vitro model of cardiac tissue, Microsc. Microanal. 11 (3) (Jun. 2005) 249–259, https://doi.org/10.1017/S1431927605050506.
[62] I. Batalov, Q. Jallerat, S. Kim, J. Bliley, A.W. Feinberg, Engineering aligned human cardiac muscle using developmentally inspired fibronectin micropatterns, Sci. Rep. 11 (1) (Jun. 2021) 1, https://doi.org/10.1038/s41598-021-87550-y.
[63] J. Malmström, et al., Large area protein patterning reveals nanoscale control of focal adhesion development, Nano Lett. 10 (2) (Feb. 2010) 686–694, https://doi.org/10.1021/nl903875r.
[64] Z. Zhao, et al., Composite hydrogels in three-dimensional in vitro models, Front. Bioeng. Biotechnol. 8 (2020), https://doi.org/10.3389/fbioe.2020.00611.
[65] H.L. Hiraki, et al., Fiber density and matrix stiffness modulate distinct cell migration modes in a 3D stroma mimetic composite hydrogel, Acta Biomater. 163 (Jun. 2023) 378–391, https://doi.org/10.1016/j.actbio.2022.09.043.
[66] M.C.T. Asuncion, J.C.-H. Goh, S.-L. Toh, Anisotropic silk fibroin/gelatin scaffolds from unidirectional freezing, Mater. Sci. Eng. C 67 (Oct. 2016) 646–656, https://doi.org/10.1016/j.msec.2016.05.087.
[67] H. Sun, et al., Biomimetic microchannel network with functional endothelium formed by sacrificial electrospun fibers inside 3D gelatin methacryloyl (GelMA) hydrogel models, J. Zhejiang Univ.-Sci. A 25 (1) (Jan. 2024) 79–96, https://doi.org/10.1631/jzus.A23D0045.
[68] L.-H. Han, J.H. Lai, S. Yu, F. Yang, Dynamic tissue engineering scaffolds with stimuli-responsive macroporosity formation, Biomaterials 34 (17) (Jun. 2013) 4251–4258, https://doi.org/10.1016/j.biomaterials.2013.02.051.
[69] J. Yang, Y. Rong, X. Chen, C. He, Hydrogel scaffolds with controlled Postgelation modulation of structures for 3D cell culture and tissue engineering, Macromol. Chem. Phys. (Dec. 2023) 2300365, https://doi.org/10.1002/macp.202300365 (vol. n/a, no. n/a).
[70] J.-H. Lee, P. Parthiban, G.-Z. Jin, J.C. Knowles, H.-W. Kim, Materials roles for promoting angiogenesis in tissue regeneration, Prog. Mater. Sci. 117 (Apr. 2021) 100732, https://doi.org/10.1016/j.pmatsci.2020.100732.
[71] J. Song, S. Gerecht, Hydrogels to recapture extracellular matrix cues that regulate vascularization, Arterioscler. Thromb. Vasc. Biol. 43 (8) (Aug. 2023) e291–e302, https://doi.org/10.1161/ATVBAHA.122.318235.
[72] F. Andriamiseza, D. Bordignon, B. Payré, L. Vaysse, J. Fitremann, 3D printing of biocompatible low molecular weight gels: imbricated structures with sacrificial and persistent N-alkyl-d-galactonamides, J. Colloid Interface Sci. 617 (Jul. 2022) 156–170, https://doi.org/10.1016/j.jcis.2022.02.076.